UNIVERSITY OF CALIFORNIA SAN DIEGO

Cosmogenic ^{35}S behavior during "double-dip" La Niña Southern Oscillation and at Solar Minimum with an application of long-term monitoring for anthropogenic ^{35}S

A thesis submitted in partial satisfaction of the requirements for the degree Master of Science

in

Chemistry

by

Valentina Engel

Committee in charge:

Professor Mark Thiemens, Chair
Professor Robert Pomeroy
Professor Jonathan H. Slade Jr.

2022

The thesis of Valentina Engel is approved, and it is acceptable in quality and form for publication on microfilm and electronically.

University of California San Diego

2022

DEDICATION

Para Humberto y Consuelo Medina por su apoyo y amor.

To my husband Stephen Engel for his unconditional love and encouragement.

EPIGRAPH

The violence that exists in the human heart is also manifest in the symptoms of illness that we see in the Earth, the water, the air, and in living things.

Pope Francis

Table of Contents

LIST OF ABBREVIATIONS

β – Beta

BDC – Brewer-Dobson Circulations

CSA – Cross-Section for Absorption

E_{max} – Maximum Energy

ENSO – El Niño Southern Oscillation

GCR – Galactic Cosmic Rays

ITCZ – Intertropical Convergence Zone

LNSO – La Niña Southern Oscillation

SPCZ – South Pacific Convergence Zone

SST – Sea Surface Temperature

STT – Stratospheric to Tropospheric Transport

ZNPP - Zaporizhzhya Nuclear Power Plant

LIST OF FIGURES

LIST OF TABLES

ACKNOWLEGEMENTS

I would like to thank Professor Mark Thiemens for his support and guidance during my time as a graduate student. I came to this program upon completion of service in the United States Navy and expressed my interest in nuclear chemistry to Professor Thiemens. My hopes were to blend my military experience as a nuclear operator with my education in chemistry and apply them to environmental research. I had received my Bachelor of Science in chemistry while living in Texas, so I did not know any of the professors at UC San Diego. I started looking through the list of professors in the Chemistry and Biochemistry department and Professor Thiemens stood out to me for his research in physical chemistry of isotope effects. Having recently completed my nuclear training, I was very familiar with radiation and isotopic behavior, so I was immediately intrigued. I sent him an email expressing interest in doing research with him and to my surprise he responded and said I might be a good fit. After meeting with him via Zoom he allowed me the opportunity to join his lab where I have learned much about isotopic behaviors in earth's environment and outside of planet earth. I have had the opportunity of working with several talented individuals who have imprinted in me a love and curiosity for environmental research that I will continue to nurture as I grow and succeed in my career.

I would like to acknowledge these inspiring individuals whom I have had the opportunity to work with during my time in the Thiemens lab and thank them for all their help and support. Thank you, Christian Boothby, Dan Crocker, Khoi Le, Jessica Gao, and Aidan King. You all have been an excellent team to work with and I appreciate all your time and dedication to this project.

I would especially like to thank Terri Jackson for her lessons and guidance during my time in the lab. Terri has been like a second mentor to me carefully guiding me through

procedures and lab protocols with upmost care and diligence. I know that I can always count on her to be there if I have a question or need assistance and she will always lend a hand. It has truly been a pleasure and an honor to work with Terri and I am eternally grateful for the lessons she has carefully taught me.

I would especially like to thank my husband Stephen for his support during this academically demanding time. Thank you for always knowing what to say when I am feeling overwhelmed and constantly motivating me to be the best version of myself that I can be. Thank you for always listening to my thoughts and pushing me to keep going even when I felt like giving up. You are my rock, and I could not have done this without you.

VITA

2018	Bachelor of Science, University of Mary Hardin-Baylor
2018-2021	United States Navy
2022	Teaching Assistant, University of California San Diego
2022	Master of Science, University of California San Diego

ABSTRACT OF THE THESIS

Cosmogenic ^{35}S behavior during "double-dip" La Niña Southern Oscillation and at Solar Minimum with an application of long-term monitoring for anthropogenic ^{35}S

by

Valentina Engel

Master of Science in Chemistry

University of California San Diego, 2022

Professor Mark Thiemens, Chair

Sulfur is one of the most interactive elements of our atmosphere, oceans, and overall biogeochemical processes. It is abundant in our oceans, sea spray aerosols, and oceanic sediments. It's presence in the atmosphere, rivers, biomass, and soils is less predominant but still significant in providing linkages between earth's major reservoirs. Since it possesses multiple valence states ranging from (-1 to +6), it can exist in a multitude of stable redox states such as carbonyl sulfide, hydrogen sulfide, elemental sulfur, or sulphate. It is because of this versatility that sulfur gains importance when studying cosmogenic production of sulfur that exists in the

atmosphere where it's behavior can provide deeper insight to atmospheric chemical processes as well as sources of changes in climate. Sulfur possesses four stable isotopic states (^{32}S, ^{33}S, ^{34}S, and ^{36}S) and one unstable nuclide (^{35}S). Radiogenic ^{35}S has a half-life of approximately 87.4 days making it an ideal tracer for atmospheric chemical evolution and dynamics. It is naturally produced by nuclear spallation of ^{40}Ar in the upper atmosphere due to high energy cosmic rays and transported down by stratospheric to tropospheric intrusions. It can also be produced by ^{35}Cl neutron capture because of thermal neutrons reacting with abundant chlorine targets in seawater. Upon decay it emits a low energy beta particle (E_{max} = 0.167 MeV), an antineutrino to conserve spin, and a ^{35}Cl atom. Due to the very low energy of the emitted beta particle and its low abundance in the atmosphere, it has not been utilized in detail until recently. By use of an ultra-low level liquid scintillation counter, it is possible to accurately detect ^{35}S in aerosol samples to track its behavior during major solar and climatic events even though the actual number of radioactive atoms is small. Solar cycle 25 and El Niño Southern Oscillations counterpart, La Niña, have major impacts on the fragile present-day climate. La Niña has been linked to several catastrophic wildfires (Shaheen et al, 2014), severe drought, and abnormal rainfall in the past and there is uncertainty when predicting this phenomenon. The production of radionuclides such as ^{35}S and ^{14}C is also altered by solar wind intensity that varies on 11-year cycles due to the sun's changing magnetic field. Combined with increased cosmic rays due to a decreased solar magnetic field, ^{35}S can afford us insight as to what is happening in the atmosphere at a deep level thus, allowing us to better prepare and adjust accordingly in response to impactful climatic events such as La Niña as well as record solar phenomena. During the time of this study, the world also witnessed the development of a Russian invasion of Ukraine. Amidst the attack on Ukraine, a nuclear power plant in southern Ukraine was targeted and overtaken by Russia on

March 4, 2022 (Castelvecchi, 2022). The Zaporizhzhya Nuclear Power Plant (ZNPP) had not reported irregular levels of radiation in the area and the damage was said to be minimal. The ZNPP is near bodies of water with high salinity making production of ^{35}S by neutron capture a possibility. Detection of irregular ^{35}S readings would be indicative of possible damage to a reactor core emitting a noticeable neutron flux. This detection method was applied following the incident that occurred at Fukushima Daiichi confirming leakage of harmful radiation and proving the extent of its reach. This method and its application will be discussed in further detail later in this study.

Chapter 1 Introduction

This introduction contains a brief overview of the production of radioactive sulfate by cosmic radiation in the atmosphere or neutron absorption in the troposphere. This description will clarify the significance of radioactive sulfate as an atmospheric tracer and identify its role in Earth's sulfur cycle. A brief description of the decay process is also included to address the radiative contribution to humans as well. The measurement of radioactive sulfate in this study has been done during a Southern Oscillation event and the start of a new Solar Cycle, a detailed overview for each phenomenon is included. This includes an explanation for Walker Circulations, Hadley Cells, and Brewer Dobson Circulations and their relevance to the present study. A brief explanation of applicable potential detection scheme for early minor neutron leaks of spent fuel canisters or active reactor cores will close this introduction.

1.1 Production and Decay of Cosmogenic ^{35}S

1.1.1 Production of Cosmogenic ^{35}S

There are 26 known isotopes of Argon on earth, three of which are stable (^{36}Ar, ^{38}Ar, and ^{40}Ar) and the most abundant being ^{40}Ar (99.6%). Argon is the third most abundant gas in the atmosphere following Nitrogen and Oxygen. As high energy cosmic rays enter and interact with the upper atmosphere, ^{40}Ar undergoes nuclear spallation to produce ^{35}S. Spallation is a nuclear process where energetic subatomic particles, such as protons, interact with an atomic nucleus (Russell et al, 1996) leading to particle evaporation and the production of an unstable nuclide. Cosmic rays, produced by solar flares or supernova explosions, are composed mostly of high energy protons traveling at approximately the speed of light. These rays bombard Earth's

atmosphere at different rates that vary in intensity and energy. Energy varies by nine orders of magnitude with the lowest being 10^9 eV. The high energy protons collide with the nucleus of an ^{40}Ar atom and a transition state period of nuclear excitation. During particle excitation, high energy protons and neutrons are emitted from the excited nucleus to shed excitation energy of the atom to a ground state. Eventually the nucleus relaxes via emission of several low energy neutrons. The product is a ^{35}S atom which rapidly oxidizes to $^{35}SO_2$ (~ 1 second) following reaction with O_2, and ultimately to sulfate aerosols by reaction with O_3, H_2O_2, or OH (Tanaka and Turekian, 1995; Turekian and Graustein, 2003). Sulfate is predominantly removed from the atmosphere by dry and wet deposition and undergoes further oxidation to produce the aerosol of interest $^{35}SO_4^{2-}$. The vast majority of ^{35}S is produced in the stratosphere and it is the only radioactive isotope that exists in the atmosphere as an aerosol and a gas simultaneously.

Another source of ^{35}S production is by ^{35}Cl absorption of thermal neutrons in seawater (Love et al, 1962). In this study, techniques were developed to detect radionuclides in oceans from reactors. This occurs as a result of primary fluid from a nuclear reactor core interacting with seawater due to a nuclear accident or undetected leak where seawater has breached the radioactive core. The primary fluid that cools the core of a nuclear reactor is rich in both fast and thermalized (lower energy) neutrons. When a reactor accident, such as the events at Fukushima, occurs there is a sudden influx of fast neutrons that escape the core. It isn't until the flux makes contact with seawater, where there is high concentration of chlorine (stable isotope ^{35}Cl; 0.55 mol/kg), that a signal of ^{35}S can be detected. In the case of Fukushima Daiichi, seawater was used an emergency coolant system providing ideal conditions for production of ^{35}S. ^{35}Cl also has a large cross section for absorption (CSA) of thermal neutrons making it an excellent candidate for neutron absorption (Sims et al, 1969). An ideal CSA combined with a high abundance in

seawater renders it a welterweight contributor to anthropogenic emission of ^{35}S into the troposphere following rapid oxidization of $^{35}SO_2$ to $^{35}SO_4^{2-}$ as occurred at Fukushima and produced the radioactive plume detected in La Jolla 5 days after admission of seawater (Priyadarshi et al, 2011). Due to the rare occurrence of reactor accidents and undetected primary leakages, in this study we focus on naturally occurring atmospheric events as sources of ^{35}S rather than neutron leakages. ^{35}S has a relatively short half-life of approximately 87.4 days, making it sensitive and of the right chronology to be utilized as a tracer for understanding and identifying stratospheric to tropospheric air mass transport on shorter time scales.

1.1.2 β^- Decay of Cosmogenic ^{35}S

There are four types of ionizing radiation: alpha, beta, neutron, and gamma in order of strength. Ionization refers to the ability of radiation to ionize atoms or molecules breaking apart crucial bonds and producing ions. Radioactive energy far exceeds bond strengths and destruction of molecules readily occurs following even minimal radiation exposure. Alpha radiation is a helium nucleus composed of two neutrons and two protons. It is commonly emitted by heavy isotopes such as ^{210}Rn and can be stopped by a standard sheet of paper, referred to as stopping distance but has energies in the MeV range. Beta radiation is defined by the emission of a charged β particle and an antineutrino or neutrino depending on the charge of the β particle. The neutrinos conserve charge in decay and are near massless. Electromagnetic radiation, such as x-ray or gamma ray radiation, is the most common radiation and the most familiar. Electromagnetic radiation is photonic, does not carry charge or mass, and energies vary depending on the source. Gamma radiation is significantly higher in energy than x-ray radiation making it much more harmful to humans and it is most attenuated when gamma sources are used

scientifically, medically, or agriculturally by lead shielding. Neutron radiation is emitted when an atom splits or fissions due to collision with a free neutron as happens in nuclear reactors. Spontaneous fission is also a possible route of decay in heavy atoms (greater than lead). This is the strongest type of radiation emitted by a chemical reaction giving different elements as products, though the process is driven by the instability of the nuclear components. Free neutrons that promote the reaction generally must first be thermalized by water in order for them to be effectively attenuated by lead shielding as they are otherwise too energetic to be stopped.

In this study, we measure beta minus radiation, the product of ^{35}S decay to its stable isotopic state, ^{35}Cl. The energy of the emitted β^- particle is very low ($E_{max} = 0.167$ MeV) making it particularly difficult to detect when there are small quantities (or activities) of the source present in a sample. Beta radiation can be attenuated by a single layer of clothing or, if contact with skin is made, will travel up to a half inch through the skin and into the body. ^{35}S, produced in the troposphere and stratosphere from neutron absorption by ^{35}Cl, is oxidized to form sulfate. It then has potential for long range transport and wet deposition into freshwater sources used for human consumption at tolerated levels of 250 mg/L according to EPA. Sulfate has sufficient transport ability that sulfate produced by biomass burning at the equator can be measured at the south pole (Shaheen et al, 2014). It plays a role in climate both cooling and warming as it nucleates clouds, which trap heat, and due to the whiteness, has a high albedo and reflects visible light and is a coolant in that process. This type of radiation can be introduced into the body in controlled amounts for treatments of cancer or medical imaging making it useful; yet when studying higher activities, must be handled with care. Its role as a clock or fingerprint of chemical and dynamical events in nature is what the thesis focuses on.

1.2 Atmospheric Southern Oscillation

Many have heard of or have been affected by the weather phenomenon referred to as an El Niño event, fewer are familiar with its counterpart, La Niña. El Niño and La Niña are the duo involved in the Southern Oscillation that occurs along the equatorial plane.

1.2.1 El Niño Southern Oscillation (ENSO)

To understand the La Niña Southern Oscillation, it is important to first understand the El Niño Southern Oscillation and the phenomena that lead to its creation. The process is inadequately known from the vantage point that it is not predictable as well as society needs to prepare for it. ENSO was given its name in the 1800's by fisherman off the Pacific Coast of South America. They began noticing that waters warmed around Christmas time some years, so they started saying that El Niño had come which means "the boy Christ-child" in Spanish. The effect that the sudden arrival of these warm waters had for the fisherman was detrimental to their livelihood and survival. They started to notice a lack of fish during these events which was due to a lack of nutrients at the surface of the ocean, product of warmer sea surface temperatures (SST). It has since been discovered that ENSO occurs due to an ocean to atmospheric coupling along the equatorial plane across the Pacific Ocean. This coupling occurs due to a constant swaying in atmospheric pressure, east to west, between the Pacific and Indian Ocean known as the Southern Oscillation (Adamson, 2020). These pressure fluctuations were later linked to temperature fluctuations (Walker Circulations) by Bjerkens (1969) who attributed the relationship to a coupling between the ocean and the atmosphere (Lau et al, 2003). He discovered positive and negative feedbacks (Bjerkens feedbacks) between trade winds and ocean sea surface temperature (SST) (Adamson, 2020). During El Niño, there is typically a weakening

in trade winds that can combine with warmer SST (+0.5˚C or greater) in the central and eastern Pacific Ocean. This combination causes increased convection above the central and eastern Pacific Ocean creating more rainfall. On the other hand, the western Pacific Ocean, typically warm with heavy rainfall, starts to become a cooler SST and less rainfall (Adamson, 2020). Since trade winds are weakened during an El Niño, the cooler water in the western Pacific is unable to upwell in the eastern Pacific causing SST to continue to rise along with convection and sea level. This is a major shift from normal conditions over the Pacific Ocean. Typically, the warm regions are the Intertropical Convergence Zone (ITCZ) (60-120˚E) and the South Pacific Convergence Zone (SPCZ) (150-90˚W) where the major area of convection lies above the maritime continent of the western tropical Pacific Ocean (Philander, 1985; Lau et al, 2003). As convection occurs over the western Pacific Ocean, low surface pressure moves the moist air towards the subtropics and the high-pressure region of the eastern Pacific Ocean where it descends (refer to Figure 1.1). Once the air cools, trade winds complete the circulation by returning the cooled air to the convective region where it warms again, and the cycle continues (Philander, 1985). This all occurs above the ocean surface. Below and at the surface there is a disruption of the normal SST preventing the cooler western Pacific water from upwelling in the eastern Pacific region. Cooled water is oxygen rich and the key to survival of marine life in the ocean. When these waters fail to upwell in the eastern Pacific due to ENSO there is miniscule amounts of oxygenated water available to produce marine life for fisherman to thrive from. ENSO is notorious for affecting socioeconomic life and causing excessive rainfall in regions that are not prepared to handle the excess volume and simultaneously creating severe drought in regions accustomed to rainfall. Weather patterns become more volatile and more extreme events that are presently unpredictable leaving countries such as South America in peril due to

aggressive floods and The Sahel in Africa in perilous drought. It is only anticipated that ENSO will become more intense as climate change continues to progress in a warm direction and its effects will follow suit.

1.2.2 La Niña Southern Oscillation (LNSO)

LNSO was discovered much later than ENSO (1980's). Its name translates to "little girl", and it was recognized as the counterpart to the known El Niño creating a cycle in the Southern Oscillation. La Niña is characterized by a temperature decrease of 0.5˚C in the El Niño 3.4 region (east central tropical Pacific between 120˚W to 170˚W longitude, defined by NOAA) while El Niño is characterized by a temperature increase of 0.5˚C, opposite of each other. El Niño and La Niña occur every 2-7 years with greater frequency of El Niño for reasons still not totally understood. During this study, data was obtained during a time of two consecutive La Niña events, or the common "double-dip", occurring 2020-2021 and 2021-2022. Characteristics of La Niña are very similar to normal non-ENSO conditions (Philander, 1985), refer to Figure 1.1, in that they do not shift the Southern Oscillation along the equator as happens during El Niño. The Southern Oscillation can be defined as a disruption in the thermally induced east to west dissemination across the Pacific Ocean known as the Walker Circulation (Chang et al, 2003) which will be discussed further in a later section. During La Niña, the oscillation is amplified, and convective forces intensify at the ITCZ while sinking from the high troposphere (~20 km) accelerates at the SPCZ (Lau et al, 2003). It is still unclear what causes this acceleration to occur, but La Niña events are attributed to either continued cooling of SST or continued strengthening of trade winds (Philander, 1985). Assuming that the cause is continued cooling of SST (opposite temperature change during El Niño) in the eastern Pacific Ocean (-

0.5˚C or lower), the gradient between the warm western Pacific and the cool eastern Pacific expands and atmospheric-oceanic interactions respond by stimulating temperature flow in order to keep up with the increasing temperature gradient across the Pacific (Philander, 1985). Warmer waters in the western Pacific enhance atmospheric convection and rainfall and the cool dry air sinking from the high troposphere (~20 km) in the eastern Pacific grows stronger (Lau et al, 2003). Deep atmospheric convection causes increased cloud coverage over Southeast Asia reducing heat from solar radiation and producing a damping effect that slows the upward atmospheric motion. To try and maintain equilibrium between the two systems, east to west trade winds intensify bringing cooled surface waters west allowing for further upwelling of deep ocean waters in the east. This reinforces the already established temperature gradient in the Pacific Ocean further increasing convection and rainfall in the west and decreasing moisture in the east. As a result, sea level rises in the ITCZ, and extreme drought overcomes the SPCZ. For the southwestern United States, this causes a significant increase in wildfires, drought, and damage to crops that is far beyond the norm. The northeastern United States is typically pummeled by abnormally heavy snowfall and rainfall putting cities at risk of severe flooding and brush overgrowth. It is important to resolve this half of the Southern Oscillation to better understand how it will behave as climate change progresses in the direction of warmer global temperatures and what the consequences for humans will be.

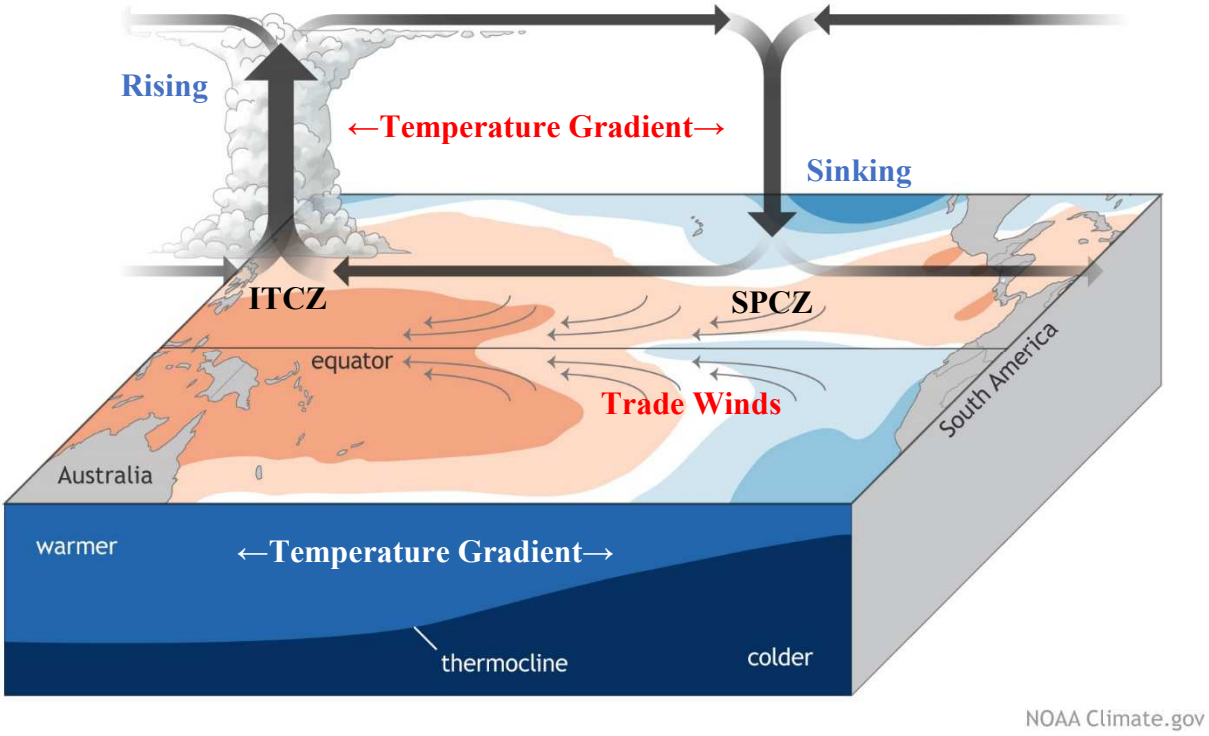

Figure 1.1 Delineation of a normal, non-ENSO, Southern Oscillation showing the regions of rising and sinking action above the Intertropical Convergence Zone (ITCZ) and the South Pacific Convergence Zone (SPCZ). [*NOAA 2021 Climate.gov*]

For this study, an issue is why does La Niña occur twice in consecutive years? In the atmosphere during a La Niña event there is a significant temperature difference between the ITCZ and the SPCZ that drives warm moist air eastward to be cooled and dried. Upon arrival in the easter Pacific, heat from the air is transferred down into the ocean continuously during a La Niña restoring the Oscillation to normal conditions. This pathlength can be followed in Figure 1.1. Of note is that there is an atmospheric upwards and downwards motion. If this is extensive, at our latitude we might expect air derived from the upper troposphere where ^{35}S levels are higher due to the proximity of the source of ^{35}S. Consequently, there is the possibility of observing radioactivity changes associated with the La Niña.

This transfer of heat is not always sufficient to warm the eastern Pacific waters enough to maintain normal conditions and thus a second La Niña ensues, and the event begins again (DiNezio et al, 2017). This “double-dip” phenomenon is common and the second La Niña is typically weaker than the first since it is more of an aftershock. After the second LNSO has passed the system should theoretically be warm enough in the eastern Pacific to prompt an ENSO, but this is a rare occurrence (DiNezio et al, 2017). Figure 1.2 demonstrates the trend of Oceanic Niño Index utilized to identify the “double-dip” La Niña that is being analyzed in this study.

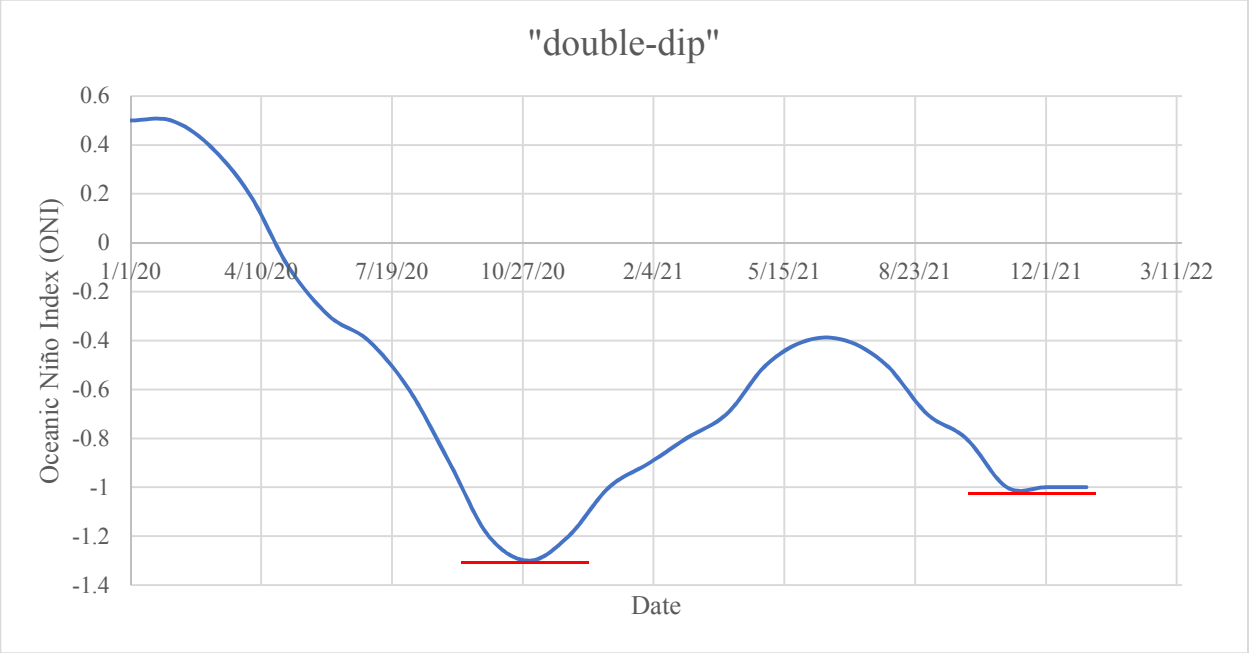

Figure 1.2 Trend of Oceanic Niño Index (ONI) beginning January 2020 through January 2022 delineating the “double-dip” phenomenon. LNSO conditions when ONI in El Niño 3.4 region is -0.5 or lower indicating the region is 0.5˚C cooler than normal (origin.cpc.ncep.noaa.gov).

Due to the unpredictable nature of La Niña and El Niño it is difficult to take measures to prepare for the detrimental conditions that accompany each event and predict if they will worsen

with progression of climate change. Improving methods of prediction and early detection can better equip affected regions and allow them to implement safety measures that allow effective responses.

1.2.3 The Walker Circulation

A key participant in the development and progression of both El Niño and La Niña is the Pacific Walker Circulation (Figure 1.1). These circulations are longitudinal winds that flow over the equatorial plane across the Pacific Ocean and are responsible for the transport of air masses within ENSO or LNSO (Liberto, 2014). They are characterized by the low-level winds that flow from the eastern Pacific to western Pacific Ocean, with convection above the ITCZ, flow back across the upper troposphere from west to east, and ultimately sink back down over the SPCZ (Liberto, 2014). These low-level winds are driven by a pressure gradient between the eastern and western Pacific waters. Low oceanic overhead atmospheric pressures in the western Pacific and high pressure in the eastern create a natural air-fluid flow from east to west. The existing potential energy in the sea resulting from the pressure and temperature gradients are transformed to kinetic energy as atmospheric air flow (Liberto, 2014). During El Niño, the Walker Circulation weakens and is shifted east such that the convergence zone moves from Southeast Asia to the eastern Pacific Ocean creating a sinking branch over the Maritime Continent. In

contrast, during La Niña there is no shift in the Walker Circulations but rather a strengthening that drives the system into deeper and stronger convection.

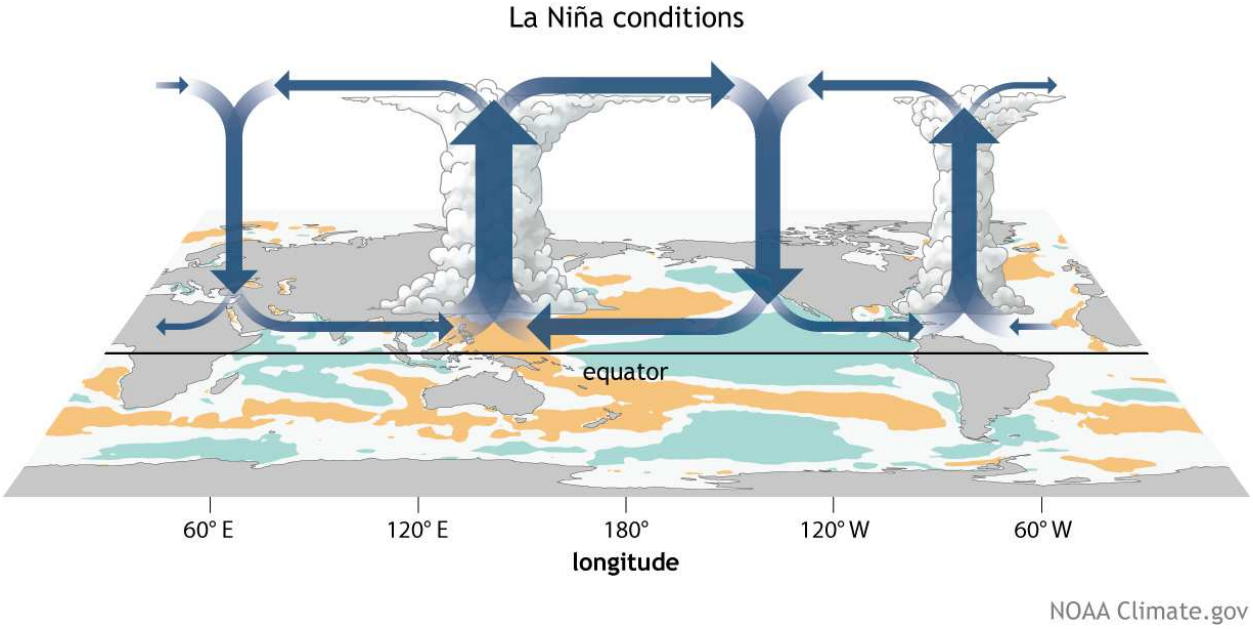

Figure 1.3 A delineation of the Walker Circulations during a La Niña Southern Oscillation [*NOAA 2021 Climate.gov*]

The Walker Circulation plays a primary role in maintaining a balance between ocean and atmospheric energies that control massive weather patterns across the equatorial plane. It's most important role as vehicle for the El Niño and La Niña Southern Oscillation.

1.2.4 Hadley Cell

An important air mass transportation system that influences stratospheric to tropospheric intrusions are the Hadley Cells. Originally postulated by English scientist George Hadley in 1735 (Warf, 2010), Hadley Cells were initially thought to be two opposing circulatory systems over each hemisphere. Hadley believed that the rising air at the equator split off into a northern and

southern direction each sinking at their respective poles and travelling back down towards the equator along the surface of the earth (Warf, 2010). It is now understood that Hadley Cells are lower latitude circulations with air masses rising at the equator and sinking at approximately 30˚ latitude in both a northern and southern direction (Rind, 1998). Since they are responsible for trade winds in the lower regions of each hemisphere, they are an important weather controller to consider when studying the La Niña Southern Oscillation. Unlike the ever-fluctuating LNSO and Walker Circulations, the Hadley Cells are constantly circulating to maintain their upward angular momentum (Angular Momentum = air mass particle × velocity of the particle × radius) as the high energy air mass particles travels up and away from the equator (Lindzen et al, 1980). The air mass travelling poleward is decreasing its distance from the earth's axis of rotation making the radius it travels around the earth progressively smaller. Since angular momentum has to be conserved and the mass of air particles cannot be changed (Lindzen et al, 1980), its eastward (westward) velocity must increase causing the air mass to stop moving poleward and begin to sink at around 30˚ north (south), depending on the cell. On the descent back down to the equator, air masses are slowed due to friction with the surface of the earth/ocean and become warmed again as they reach the equator. The sinking motion of the Hadley Cell creates areas of high pressure off the coast of California and over the islands of Bermuda known as the Pacific and the Bermuda Highs, respectively (Warf, 2010). These high-pressure regions, particularly the Pacific High, prevent the formation of clouds and precipitation. For Southern California this equates to a more intense drought when combined with the effects of the La Niña Southern Oscillation. During the poleward travel of air masses in the Hadley Cell, it is probable that at heights of approximately 15-17 km, particles, such as cosmogenic ^{35}S, from the sub stratosphere can become entrained and brought down to the troposphere. Combined with accelerated Walker

circulations during La Niña, the likelihood of seeing more frequent spikes in upper tropospheric-stratospheric cosmogenic ^{35}S increases. Along with this are occurrences of high-pressure events creating extreme dryness from the stratospheric air mass admixture.

1.2.5 Brewer-Dobson Circulations

Brewer-Dobson Circulations (BDC) affect the entire globe by admitting tropospheric air up into the stratosphere and circulating it poleward before sinking back down at mid (30˚) or high (60˚) latitudes (Butchart, 2014). BDC are meridional cells in the upper and lower hemisphere (Fu et al, 2019) similar to the Hadley Cells. They extend larger distances and reach altitudes of up to 70 km (Butchart, 2014) creating stratospheric to tropospheric mixing events. They are responsible for entraining air from the tropical tropopause layer (TTL) and moving it poleward until it sinks into the troposphere at mid to high latitudes carrying stratospheric ozone and radioactive isotopes such as cosmogenic ^{35}S. BDC play a vital role in tropospheric chemistry directly affecting the levels of O_3 in the troposphere and influence the oxidative capacity of the troposphere (Butchart, 2014). The oxidative capacity of the troposphere from the presence of ozone is what dictates the evolution of aerosols that contain cosmogenic sulfate and the lifetime of long-lived gases (Kentarchos and Roelofs, 2003). Stratospheric to tropospheric transport (STT) of air masses can largely be attributed to Brewer-Dobson Circulations. However, it is possible that the combination of BDC, Walker Circulations, and the Hadley Cell can develop a greater likelihood of deep STT in the eastern Pacific Ocean region and Southern California during certain times of year. Studies of the impact of deep STT on the tropospheric sulfur cycle are scarce but further research could give insight on the effects of STT on tropospheric sulfur

cycle and ozone levels given the suitable half-life of ^{35}S and the newest observations of the processes (Lin et al, 2016c).

1.3 Solar Minimum of Solar Cycle 25

Solar Cycle 25 was officially announced in December 2019 after observing the lowest point of the solar minimum between Solar Cycle 24 and 25 (NOAA, 2020). During a solar minimum there is a weakening of solar magnetic field that allows for a greater flux of galactic cosmic rays (GCR) to arrive at Earth's atmosphere (Rahmanifard et al, 2021). GCR are produced by massive explosive events such as supernova or, in the case of the Sun, solar flares accompanied by coronal mass ejections. During a solar minimum the presence of a weaker magnetic field is accompanied by fewer sunspots. Therefore, the solar flares that are produced around sunspots, though fewer, are more likely to reach earth's atmosphere at higher intensity due to the weaker magnetic field. They are composed of high energy particles such as protons, heavy ions, and electrons (Rahmanifard et al, 2021) with the majority being high energy protons. This increased flux of GCR increases the rate of argon spallation in the upper atmosphere directly increasing the production rate for several radioisotopes, which includes ^{35}S and ^{14}C. The production of cosmogenic ^{35}S increases and due to its suitable half-life of approximately 87 days, is an ideal tracer that can be used to detect changes in solar activity rapidly and in a different way from conventional solar observations, both land and satellite based. Unlike ^{14}C and ^{10}Be, which are used as long-term tracers to understand solar activity back as far as 10,000 years (Rahmanifard et al, 2021), we use ^{35}S to see changes in solar activity happening on a much shorter time scale given its 87-day half-life. Current investigations regarding the possibility of a secular, or slow moving, solar minimum at the start of solar cycle 25 is being carried out using historical data and technological imaging. It is possible that ^{35}S could yield useful information in

conjunction with these methods for a better understanding of present solar conditions since concentrations of ^{35}S will fluctuate proportionately with GCR intensity. During a solar minimum GCR intensity will be greater and therefore an increase in ^{35}S should be detectable. NASA has gained an increased interest in space weather prediction due to upcoming projects such as Artemis that will expose spacecraft and astronauts to long term space radiation (Potter, 2021). It is imperative that space weather prediction become as efficient as meteorological predictions on earth for the safety and well-being of the people and equipment used for these explorations. The effects of GCR also have a potential impact on earth's atmosphere, this facilitates a deeper understanding for solar and space interactions with the earth's atmosphere and potential consequences.

1.4 Detection of ^{35}S Produced by Neutron Fluxes

Production of ^{35}S may result from thermal neutron capture by highly abundant ^{35}Cl in seawater (Love et al, 1962). $^{35}Cl[n,p]^{35}S$ has an ideal cross section for absorption of 0.40 ± 0.01 barns for thermal neutrons (Sims et al, 1969) making it the most likely reaction pathway if there is neutron leakage into the ocean. ^{35}S can also be produced by $^{34}S\ [n,\gamma]^{35}S$ but this reaction is 200 times less likely to occur than the thermal neutron absorption by ^{35}Cl as described earlier (Love et al 1962). On March 4, 2022, the Zaporizhzhya Nuclear Power Plant (ZNPP) in Ukraine was bombarded by Russian forces (Castelvecchi, 2022). The use of explosive weapons resulted in damage to several components at ZNPP placing the integrity of the reactor vessels in question. The Zaporizhzhya Nuclear Power Plant (ZNPP) had not reported irregular levels of radiation in the area following the attack and damage was said to be relatively minor (Castelvecchi, 2022). Given that the ZNPP is in close proximity to the Black Sea, the Sea of Azov, and the Caspian

Sea, production of ^{35}S by neutron capture is not out of the question. Neutron leakage from damage to ZNPP cooling systems or control systems could result in a reactor accident similar to that of Fukushima Daiichi (Castelvecchi, 2022) causing neutron leakage into the sea as a result of seawater use as an emergency coolant system. Since very little reporting has been made concerning the actual damage to the facility, it is difficult to completely rule out the possibility of neutron leakage from cooling or control systems that may have been damaged at the facility during the attack. Given prevailing air mass trajectories and distance, it is unlikely that a signal would be detected here as compared to Fukushima where the air mass trajectory at that time was a 5-day transit to La Jolla. Historical accidents such as the occurrence at Chernobyl and Fukushima Daiichi have demonstrated the profound impact that a release of harmful radiation into the environment can have. The danger posed to human health and the surrounding ecology by accidents of this nature are more than enough reason to take damage to nuclear facilities seriously and investigate even the most minute possibility of neutron leakage. On the southern coast of California near one of the most popular surfing locations in country is the San Onofre Nuclear Generating Station (SONGS). SONGS has become the new home to 3.55 million pounds of spent fuel contained in steel canisters that are classified as radioactive waste (Nikolewski, 2019). Spent fuel canisters previously kept in wet storage pools have been relocated to a dry storage facility at SONGS where they are set to remain for an indefinite period of time. It is important to keep in mind that these structures are vulnerable to chloride induced stress corrosion cracking (CISCC) as a result of their location. Damage to a containment structure could result in the release of neutron radiation which would be harmful to humans and the ecology. This is only one example of the many nuclear power generating stations that exist in the country. Several other nuclear power plants in the United States are also located near large

bodies of saline water such as SONGS is to the Pacific Ocean. Existing methods of radiation detection are effective, and it would only be beneficial to add layers of security to keep nearby populations safe. By use of ^{35}S, neutron leakage could quickly be detected, and the site notified immediately upon confirmation that the source of abnormally high ^{35}S can be attributed to a neutron leak. Prompt action would allow neighboring cities to implement safety precautions and prepare people for safe evacuation if necessary. The nuclear facility would have time to detect the source of leakage and contain it before worsening conditions ensued. It is possible that a small undetected fracture could begin to leak unnoticed and then become severely aggravated over time or due to unpredictable weather events that would escalate the danger significantly. By constantly monitoring levels of ^{35}S and understanding its behavior during normal weather conditions in the region, it would be easier to detect an abnormal level. Levels out of normal range could then be traced back to their origin using NOAA HYSPLIT technology to confirm whether or not the ^{35}S originated in the atmosphere or from a nuclear facility.

1.5 Motivation for Thesis

The sulfur cycle has the potential to serve as a useful tool to better understand several complex phenomena related to weather and solar activity in the earth's environment. The purpose of this thesis is to better understand the behavior of ^{35}S with respect to transients in climate and solar activity and take advantage of a La Niña event occurring and providing a perturbation to normal conditions. Also, to describe the usage of ^{35}S as a low cost and long-term radiation safety detection method that can be implemented near nuclear power generating stations.

This analysis will provide insight for three significant scientific questions: (1) Can cosmogenic ^{35}S be used as a tracer to indicate the presence or intensity of a La Niña Southern

Oscillation? (2) Can cosmogenic ^{35}S behavior be used to develop a better understanding of solar transitions and cycle activity? (3) Can anthropogenic ^{35}S be used long term to detect early signs of damage to nuclear power generating stations or nuclear waste storage facilities?

Chapter 2 Results and Discussion

2.1 Behavior of Cosmogenic ^{35}S during a "double-dip" La Niña Southern Oscillation

Sulfate aerosols can act as cloud condensation nuclei (CCN), also known as cloud seeds, and reflect solar radiation making them a key component to climate systems around the world (Shaheen et al, 2013). Some geoengineering experiments suggest admitting sulfate into the atmosphere to form clouds for reflection of incoming solar rays enhancing its cooling effect as a CCN (Robock, 2003). Cosmogenic ^{35}S produced in the stratosphere interacts with ozone, hydrogen peroxide, or hydroxide and rapidly oxidizes to sulfur dioxide (~1 second) which continues to react with ozone becoming a sulfate aerosol particle. Sulfate is a pollutant that can be detrimental to climate, agriculture, and human health (Unger, 2006). It has the opposite effect on climate when compared to most greenhouse gases and common pollutants in that it causes a cooling effect rather than a warming effect (Unger, 2006). During the study we collected sulfate aerosols of different sizes (>1.5 μm, <0.95 μm, and in between) to encompass a broad range of data and to enhance resolution within each range for differentiation chemistries of particle origin. Particles >1.5 μm constitute bulk sulfate aerosol samples, <1.5 μm but >0.95 μm constitute coarse sulfate aerosol samples, and <0.95 μm constitute fine sulfate aerosol samples (Lin et al, 2016c; Brothers et al 2010). Bulk samples contain sulfate aerosols that have undergone particle growth reactions during stratospheric to tropospheric transport (STT). Coarse and fine samples combined account for the bulk sample and their separation may help us identify particles that are potentially anthropogenically produced by neutron absorption. Focusing on bulk and fine aerosol samples the behavior of sulfate will be analyzed during the 2020-2021 and subsequent 2021-2022 La Niña Southern Oscillation ("double-dip") to provide a unique perspective on atmospheric changes during this complex weather phenomenon that is yet to be fully understood.

Table 1.1 Bulk Radiosulfate Concentration and Humidity during 2020-2021 La Niña Southern Oscillation

Bulk Sample Name	*Date Range*	*DPM*	*Radiosulfate Concentration (atoms m^{-3})*	*Humidity*
UH113b S35 1/2	7/30-8/7/2020	8.388	282.564	76.82
UH114b S35 1/2	8/7-8/14/2020	11.452	451.013	68.54
UH114b S35 1/2	8/7-8/14/2020	5.338	309.917	68.54
UH115b S35 1/2	8/14-8/21/2020	7.595	282.154	46.38
UH116b S35 1/2	8/21-8/27/2020	4.402	184.844	65.37
UH117b S35 1/2	8/27-9/8/2020	27.795	588.974	72.88
UH117b S35 1/2	8/27-9/8/2020	27.883	600.275	72.88
UH117b S35 1/2	8/27-9/8/2020	15.395	444.307	72.88
UH118b S35 1/2	9/8-9/11/2020	5.234	428.013	77.48
UH119b S35 1/2	9/11-9/14/2020	6.349	497.210	59.08
UH119b S35 1/2	9/11-9/14/2020	4.891	463.186	59.08
UH120b S35 1/2	9/14-9/17/2020	5.866	468.324	72.17
UH121b S35 1/2	9/17-9/21/2020	3.739	266.076	32.66
UH122b S35 1/2	9/21-9/25/2020	4.284	294.093	74.75
UH123b S35 1/2	9/25-9/28/2020	5.442	454.941	75.89
UH124b S35 1/2	9/28-10/2/2020	8.248	490.571	73.68
UH125b S35 1/2	10/2-10/6/2020	5.771	393.503	74.75
UH126b S35 1/2	10/6-10/9/2020	6.602	528.159	59.21
UH127b S35 1/2	10/9-10/12/2020	3.815	305.026	67.08
UH128b S35 1/2	10/12-10/16/2020	5.641	342.186	63.82
UH129b S35 1/2	10/16-10/20/2020	4.302	264.961	55.49
UH130b S35 1/2	10/20-10/23/2020	3.271	275.330	75.6
UH131b S35 1/2	10/23-10/27/2020	12.044	675.850	64.08
UH132b S35 1/2	10/27-10/30/2020	6.634	568.008	26.07
UH133b S35 1/2	10/30-11/3/2020	6.724	427.223	56.55
UH134b S35 1/2	11/03-11/6/2020	4.016	325.311	81.58
UH135b S35 1/2	11/06-11/10/2020	4.848	317.538	78.06
UH136b S35 1/2	11/11-11/14/2020	3.449	316.248	58.17
UH137b S35 1/2	11/14-11/17/2020	4.086	295.769	71.38
UH138b S35 1/2	11/17-11/20/2020?	2.675	209.351	44.1
UH139b S35 1/2	11/20-11/24/2020	3.189	249.318	75.67
UH140b S35 1/2	11/24-11/28/2020	4.119	304.821	70.84
UH141b S35 1/2	11/28-12/01/2020	5.308	392.718	31.59
UH142b S35 1/2	12/1-12/4/2020	7.539	571.232	35.68
UH143b S35 1/2	12/4-12/7/2020	10.161	802.416	35.37
UH144b S35 1/2	12/7-12/10/2020	4.712	470.974	46.62
UH145b S35 1/2	12/10-12/14/2020	5.755	388.837	64.93
UH146b S35 1/2	12/14-12/17/2020	3.159	316.913	74.83

Table 1.1 Bulk Radiosulfate Concentration and Humidity during 2020-2021 La Niña Southern Oscillation (Continued).

UH147b S35 1/2	12/17-12/21/2020	4.026	268.671	66.98
UH148b S35 1/2	12/21-12/24/2020	4.379	349.339	39.03
UH149b S35 1/2	12/24-12/28/2020	7.266	447.309	24.77
UH150b S35 1/2	12/28-12/31/2020	2.269	199.633	77.94
UH151b S35 1/2	12/31-1/4/2021	3.415	228.442	68.91
UH152b S35 1/2	1/4-1/7/2021	1.951	190.346	81.71
UH153b S35 1/2	1/7-1/11/2021	4.071	322.031	73.07
UH154b S35 1/2	1/11-1/14/2021	4.468	433.932	40.59
UH155b S35 1/2	1/14-1/18/2021	5.675	408.797	34.27
UH156b S35 1/2	1/18-1/21/2021	2.518	275.271	57.62
UH157b S35 1/2	1/21-1/25/2021	5.386	304.029	69.14
UH158b S35 1/2	1/25-1/28/2021	2.222	229.903	64.34
UH159b S35 1/2	1/28-2/1/2021	2.504	192.458	62.2
UH160b S35 1/2	2/1-2/4/2021	1.851	177.846	55.91
UH161b S35 1/2	2/4-2/8/2021	6.195	474.511	74.47
UH162b S35 1/2	2/8-2/11/2021	6.906	628.610	76.33
UH163b S35 1/2	2/11-2/15/2021	3.532	280.750	75.97
UH164b S35 1/2	2/15-2/18/2021	2.821	296.485	72.66
UH165b S35 1/2	2/18-2/22/2021	3.594	281.429	41.94
UH166b S35 1/2	2/22-2/25/2021	4.456	454.988	30.57
UH167b S35 1/2	2/25-3/1/2021	8.461	762.075	54.19
UH168b S35 1/2	3/1-3/4/2021	4.332	518.540	28.76
UH169b S35 1/2	3/4-3/8/2021	4.535	386.845	74.31
UH170b S35 1/2	3/8-3/11/2021	2.029	223.754	72.34
UH171b S35 1/2	3/11-3/15/2021	4.313	388.643	68.37
UH172b S35 1/2	3/15-3/18/2021	2.451	286.076	67.45
UH173b S35 1/2	3/18-3/22/2021	3.149	272.783	73.74
UH174b S35 1/2	3/22-3/25/2021	3.061	328.003	65.65
UH175b S35 1/2	3/25-3/29/2021	4.856	372.905	74.59
UH176b S35 1/2	3/29-4/1/2021	8.114	868.508	59.41
UH177b S35 1/2	4/1-4/5/2021	10.826	861.970	30.42
UH178b S35 1/2	4/5-4/8/2021	6.476	657.196	74.62
UH179b S35 1/2	4/8-4/12/2021	8.114	714.998	73.02
UH180b S35 1/2	4/12-4/15/2021	7.593	820.102	65.3
UH181b S35 1/2	4/15-4/19/2021	9.354	764.623	59.89
UH182b S35 1/2	4/19-4/22/2021	6.487	640.122	42.62
UH183b S35 1/2	4/22-4/26/2021	4.676	393.855	74.32
UH184b S35 1/2	4/26-4/29/2021	2.941	303.280	71.31
UH185b S35 1/2	4/29-5/3/2021	5.327	437.149	42.99
UH186b S35 1/2	5/3-5/6/2021	3.327	343.988	69.89

Table 1.1 Bulk Radiosulfate Concentration and Humidity during 2020-2021 La Niña Southern Oscillation (Continued).

UH187b S35 1/2	5/6-5/10/2021	8.114	601.171	71.88
UH188b S35 1/2	5/10-5/14/2021	7.110	556.894	67.29
UH189b S35 1/2	5/14-5/17/2021	2.507	258.429	69.78
UH190b S35 1/2	5/17-5/20/2021	2.301	223.076	74.64
UH191b S35 1/2	5/20-5/24/2021	3.649	266.195	68.69
UH192b S35 1/2	5/24-5/27/2021	3.204	354.960	64.93
UH193b S35 1/2	5/27-5/30/2021	3.477	380.487	65.58

Table 1.2 Bulk Radiosulfate Concentration and Humidity during 2021-2022 La Niña Southern Oscillation

Bulk Sample Name	*Date Range*	*DPM*	*Radiosulfate Concentration (atoms m^{-3})*	*Humidity*
UH211b S35 1/2	8/1-8/5/2021	6.659	511.504	67.13
UH212b S35 1/2	8/5-8/10/2021	6.351	373.624	76.3
UH213b S35 1/2	8/10-8/13/2021	3.494	385.388	75.01
UH214b S35 1/2	8/13-8/17/2021	6.296	435.950	61.83
UH215b S35 1/2	8/17-8/20/2021	3.323	357.550	76.77
UH216b S35 1/2	8/20-8/23/2021	6.899	713.325	72.14
UH217b S35 1/2	8/23-8/26/2021	5.069	500.665	70.08
UH218b S35 1/2	8/26-8/30/2021	4.423	333.573	64.88
UH219b S35 1/2	8/30-9/2/2021	6.194	592.299	78
UH220b S35 1/2	9/2-9/7/2021	7.863	442.877	68.03
UH221b S35 1/2	9/7-9/10/2021	4.640	409.155	74.42
UH222b S35 1/2	9/10-9/14/2021	5.353	362.840	74.52
UH223b S35 1/2	9/14-9/17/2021	9.580	916.970	76.26
UH224b S35 1/2	9/17-9/20/2021	8.904	790.741	68.84
UH225b S35 1/2	9/20-9/23/2021	3.353	324.888	74.95
UH226b S35 1/2	9/23-9/27/2021	7.351	506.462	73.41
UH227b S35 1/2	9/27-9/30/2021	3.766	333.154	84.29
UH228b S35 1/2	9/30-10/4/2021	8.023	538.019	68.07
UH229b S35 1/2	10/4-10/7/2021	5.763	476.422	43.56
UH230b S35 1/2	10/7-10/11/2021	4.221	290.187	79.47
UH231b S35 1/2	10/11-10/14/2021	4.739	437.003	73.79
UH232b S35 1/2	10/14-10/18/2021	8.153	562.323	56.65
UH232b S35 1/2	10/14-10/18/2021	6.031	487.419	56.65
UH233b S35 1/2	10/18-10/21/2021	3.966	342.397	74.61
UH234b S35 1/2	10/21-10/25/2021	5.269	358.310	75.14

Table 1.2 Bulk Radiosulfate Concentration and Humidity during 2021-2022 La Niña Southern Oscillation (Continued).

UH236b S35 1/2	10/25-10/28/2021	3.739	314.843	81.85
UH238b S35 1/2	10/18-11/1/2021	2.624	170.574	47.01
UH240b S35 1/2	11/1-11/4/2021	2.151	173.931	79.7
UH242b S35 1/2	11/4-11/8/2021	3.699	246.284	83
UH244b S35 1/2 (UG)	11/8-11/12/2021	4.704	313.328	79.4
UH244b S35 1/2 (IG)	11/8-11/12/2021	3.663	242.039	79.4
UH246b S35 1/2 (UG)	11/12-11/16/2021	3.090	198.878	32.12
UH248b S35 1/4 (IG)	11/16-11/19/2021	1.910	312.554	83.42
UH248b S35 1/4 (UG)	11/16-11/19/2021	2.120	349.678	83.42
UH250b S35 1/2 (UG)	11/19-11/24/2021	6.856	339.383	81.03
UH252b S35 1/2 (UG)	11/24-11/29/2021	4.290	529.436	75.58
UH254b S35 1/2 (UG)	11/29-12/2/2021	3.970	311.945	52.68
UH256b S35 1/2 (UG)	12/2-12/6/2021	6.480	390.554	86.59
UH258b S35 1/2 (UG)	12/6-12/9/2021	5.790	496.552	83.98
UH260b S35 1/2 (UG)	12/9-12/13/2021	7.286	528.340	85.79
UH262b S35 1/2 (UG)	12/13-12/16/2021	4.030	392.717	75.98
UH264b S35 1/2 (UG)	12/16-12/20/2021	3.853	259.395	74.71
UH266b S35 1/2 (UG)	12/20-12/23/2021	4.120	387.605	68.94
UH268b S35 1/2 (UG)	12/23-12/28/2021	3.680	220.043	74.35
UH270b S35 1/2 (UG)	12/28-12/31/2021	0.756	67.840	80.6
UH272b S35 1/2 (UG)	12/31-1/4/2022	7.081	487.536	75.91
UH274b S35 1/2 (UG)	1/4-1/7/2022	5.249	452.2563	77
UH276b S35 1/2 (UG)	1/7-1/12/2022	6.74	355.5634	85
UH278b S35 1/2 (UG)	1/12-1/15/2022	6.42	546.2036	37
UH280b S35 1/2 (UG)	1/15-1/18/2022	6.787	581.0315	59
UH282b S35 1/2 (UG)	1/18-1/21/2022	3.813	315.5618	87
UH284b S35 1/2 (UG)	1/21-1/25/2022	4.451	328.273	73
UH286b S35 1/2 (UG)	1/25-1/28/2022	5.224	456.514	75
UH288b S35 1/2 (UG)	1/28-2/1/2022	9.124	576.3968	42
UH290b S35 1/2 (UG)	2/1-2/4/2022	7.139	579.2065	76
UH292b S35 1/2 (UG)	2/4-2/8/2022	5.664	365.1155	45
UH294b S35 1/2 (UG)	2/8-2/11/2022	3.454	296.1787	26
UH296b S35 1/2 (UG)	2/11-2/14/2022	3.179	266.6124	33
UH298b S35 1/2 (UG)	2/15-2/18/2022	4.466	377.8431	75
UH300b S35 1/2 (UG)	2/18-2/22/2022	6.316	426.9875	48
UH302b S35 1/2 (UG)	2/22-2/25/2022	3.603	291.9075	74

Table 1.1 and Table 1.2 contain radiosulfate concentrations within the time frame designated by the National Oceanic and Atmospheric Administration (NOAA) to be LNSO. An SST in the negative region (starting at -0.5˚C and decreasing) is used to indicate the presence of LNSO as can be seen in Table 1.3 (nws.noaa.gov). Radiosulfate concentrations collected during LNSO months along with humidity were plotted against dates of collection which trend lower in Southern California during LNSO due to sinking of dried air transported from ITCZ via Walker Circulations.

During 2020-2021 LNSO and 2021-2022 LNSO aerosol sulfate was collected, extracted, purified, and counted for recording following protocol delineated by Brothers et al (2010) and Lin et al (2017b). Samples were regularly collected on the fifth floor of Urey Hall at the University of California in La Jolla starting in May of 2019. Data presented in Table 1.1 and Table 1.2 encompasses the 2020-2021 and subsequent 2021-2022 LNSO and includes humidity data corresponding to the time frame for when each sample was collected (Visual Crossing Weather).

La Niña events are known to alter weather patterns and affect humidity at its convergence zones; exponentially increasing humidity at the ITCZ and decreasing humidity at the SPCZ drastically. This variation in humidity can be connected back to the behavior of Walker Circulations during the LNSO. Moving at an accelerated rate during LNSO, dry air sinks down at the equatorial SPCZ and rises again as it is transported poleward north and south by the Hadley Cells and BDC. With humidity decreasing at the SPCZ, hot dry air begins to rise at the equatorial level within the Hadley Cell and BDC where it ultimately sinks back down at approximately 30˚ north and south of the equator (Rind, 1998). Focusing on the northern hemisphere, La Jolla California is located at approximately 32˚ N which includes it in the high-

pressure region of downward air transport of the Hadley Cells and BDC, where stratospheric injections are maximal. The weather conditions in Southern California become dryer beginning in the fall and last through the winter matching the seasonal time frame for LNSO. Sulfate aerosols can be removed from the atmosphere by dry or wet deposition but typically remain in solid form while humidity levels are below 80% (Kirpes et al, 2022). During high pressure events resulting from transported air masses of the Hadley Cell and BDC, STT events entrain sulfate aerosols which undergo particle growth interactions as they sink down into the troposphere. Bulk samples collected containing sulfate aerosol particles of greater than 1.5µm were plotted along with humidity against date to observe behavior during non-ENSO conditions and compare them to LNSO conditions.

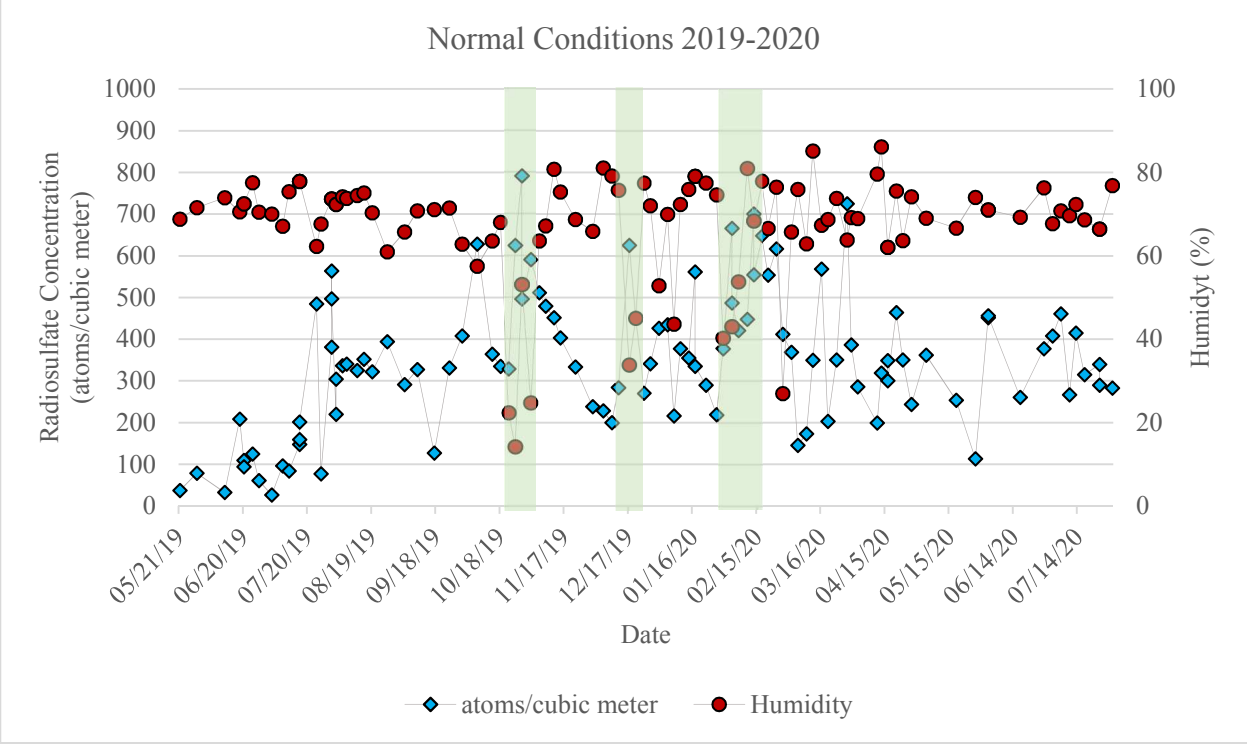

Figure 1.4 Bulk radiosulfate concentration and humidity plotted against date during non-ENSO Conditions in 2019-2020. Instances highlighted where radiosulfate concentration exceeds 600 atoms m^{-3} accompanied humidity below 60% indicative of a stratospheric event.

During normal ENSO conditions, elevated concentrations of radiosulfate can be seen within the fall to spring seasonal timeframe due to the presence of high-pressure events and occurrence Santa Ana winds popular to Southern California. Humidity seldom fluctuates significantly out of an 80-60% range during non-ENSO conditions as well. Figure 1.4 delineates normal (non-ENSO) conditions from 2019-2020 which are characterized by NOAA as having SST temperature change less than 0.5˚C but greater than -0.5˚C, values referred to as an Oceanic Niño Index (ONI). Table 1.3 contains ONI values encompassing this study where values in red indicate warming SST and values in blue indicate cooling SST.

Table 1.3 Monthly Oceanic Nino Index (ONI) beginning 2019 last updated March 31, 2022. LNSO conditions when ONI in El Niño 3.4 region is -0.5 or lower indicating the region is 0.5˚C cooler than normal (NOAA)

Oceanic Nino Index				
	2019	2020	2021	2022
January	0.7	0.5	-1	-1
February	0.7	0.5	-0.9	
March	0.7	0.4	-0.8	
April	0.7	0.2	-0.7	
May	0.5	-0.1	-0.5	
June	0.5	-0.3	-0.4	
July	0.3	-0.4	-0.4	
August	0.1	-0.6	-0.5	
September	0.2	-0.9	-0.7	
October	0.3	-1.2	-0.8	
November	0.5	-1.3	-1	
December	0.5	-1.2	-1	

During normal conditions, or non-ENSO conditions, there are greater instances during autumn and winter where bulk concentrations of radiosulfate rise above 600 atoms m^{-3}. These spikes in concentration are accompanied by significant drops in humidity which are indicative of

high-pressure events leading to STT of large sulfate aerosol particles entrained in downward air mass transport. This illustrates the effectiveness of defining the natural processes that alter ^{35}S as shown by Lin et al (2022), in southern California El Niño events.

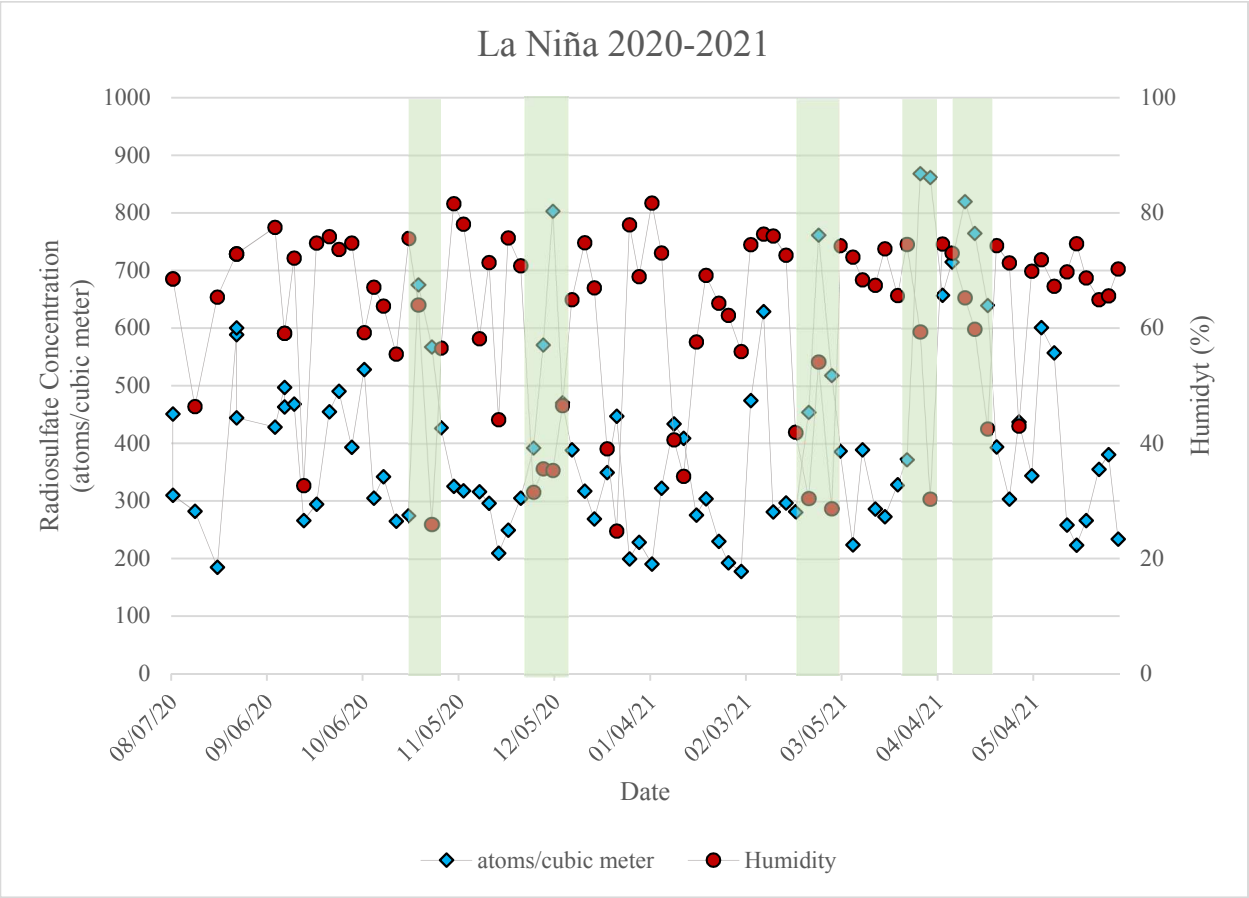

Figure 1.5 Bulk radiosulfate concentration and humidity plotted against date during LNSO Conditions 2020-2021. Instances highlighted where radiosulfate concentration exceeds 600 atoms m^{-3} accompanied humidity below 60%.

The 2020-2021 LNSO contains more frequent stratosphere to troposphere intrusions when compared to non-ENSO conditions of Figure 1.4. During 2020-2021 LNSO conditions, humidity fluctuates more drastically when compared to non-ENSO conditions. This is clearly

shown when comparing Figures 1.4 and 1.5. More frequent periods of low humidity indicate a decrease in rainfall which further aggravates the existing drought conditions in Southern California and the rest of the southwestern regions of the country. During instances of low humidity, cosmogenic radiosulfate is more successfully transported down to the troposphere where aerosols can be collected and analyzed. When there is less washout of particulate sulfate aerosol from the atmosphere, a more definite picture of upper atmospheric behavior can be generated, and a better understanding of sulfur cycle and ozone budget trajectory can be obtained. LNSO typically appears in autumn and lasts into spring overlapping with Santa Ana wind season in Southern California. Santa Ana winds originate in inland deserts primarily centered over Nevada. The high-pressure divergence then forcing its way along the surfaces and through the coastal mountains towards the coast of California (Lin et al, 2022d) is a significant influence on ^{35}S concentrations during non-ENSO conditions. This study indicates there is a correlation between increased STT events and LNSO combined with Santa Ana wind frequency. Data from this project provides the first examination of ^{35}S behavior during an individual La Niña events as well as a single "double-dip" La Niña event in which two LNSO occur consecutively. Figure 1.6 will show the brief period between LNSO 2020-2021 and LNSO 2021-2022 can be considered to be non-ENSO conditions. Due to the short timeframe, LNSO 2021-2022 will be compared to non-ENSO conditions from 2019-2020 which includes typical LNSO months.

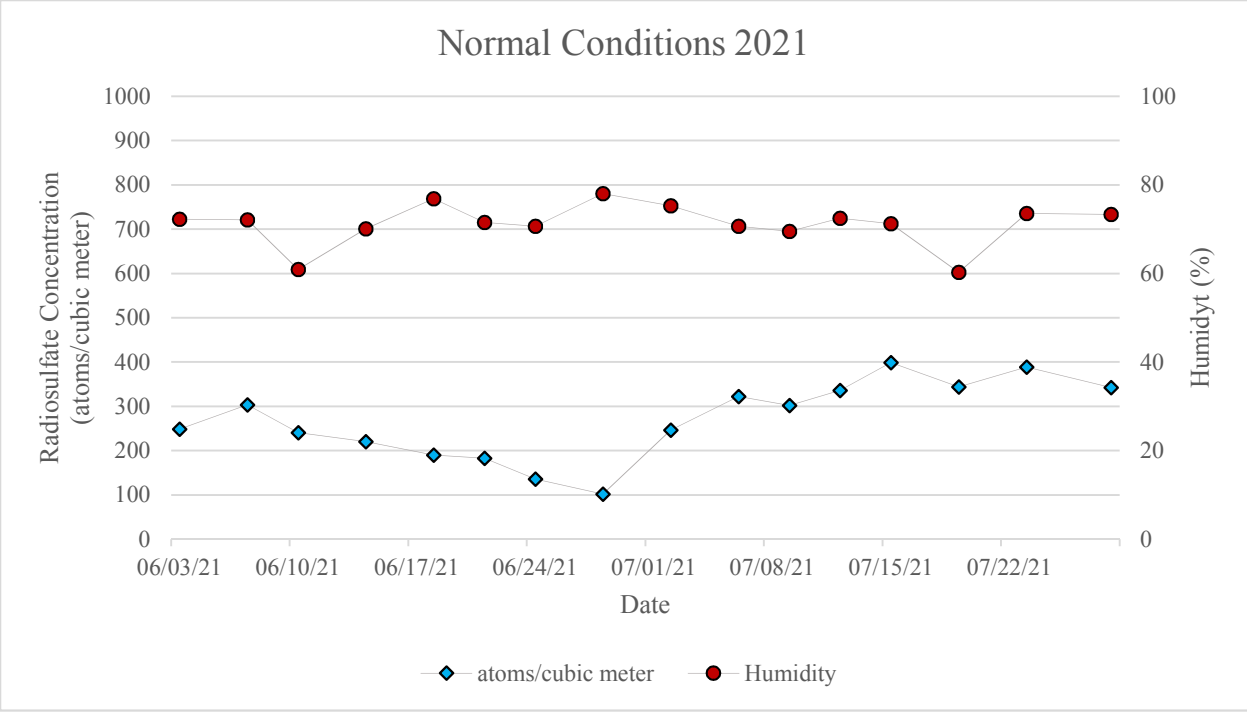

Figure 1.6 Bulk radiosulfate concentration and humidity plotted against date during brief non-ENSO Conditions 2021 leading up to a second LNSO event.

During summer months STT events are rare and Santa Ana winds do not occur, therefore spikes in radiosulfate are not seen during this time. This short period of time between LNSO 2020-2021 and LNSO 2021-2022 demonstrated an upward trend of radiosulfate concentration beginning July of 2021 where an ONI of -0.4˚C was reported by NOAA for the month of June and July of 2021 (reference table 1.3). This increasing concentration of ^{35}S could serve as a clear indication that a second LNSO event will occur and could be used in conjunction with meteorological and Pacific Ocean satellite SST observations to confirm on earlier time scale predictions of a second La Niña. It is important to analyze climate behavior since there is a potential influence from the changing solar cycle that could alter levels of ^{35}S as well given that these measurements are during a deep and protracted solar minima.

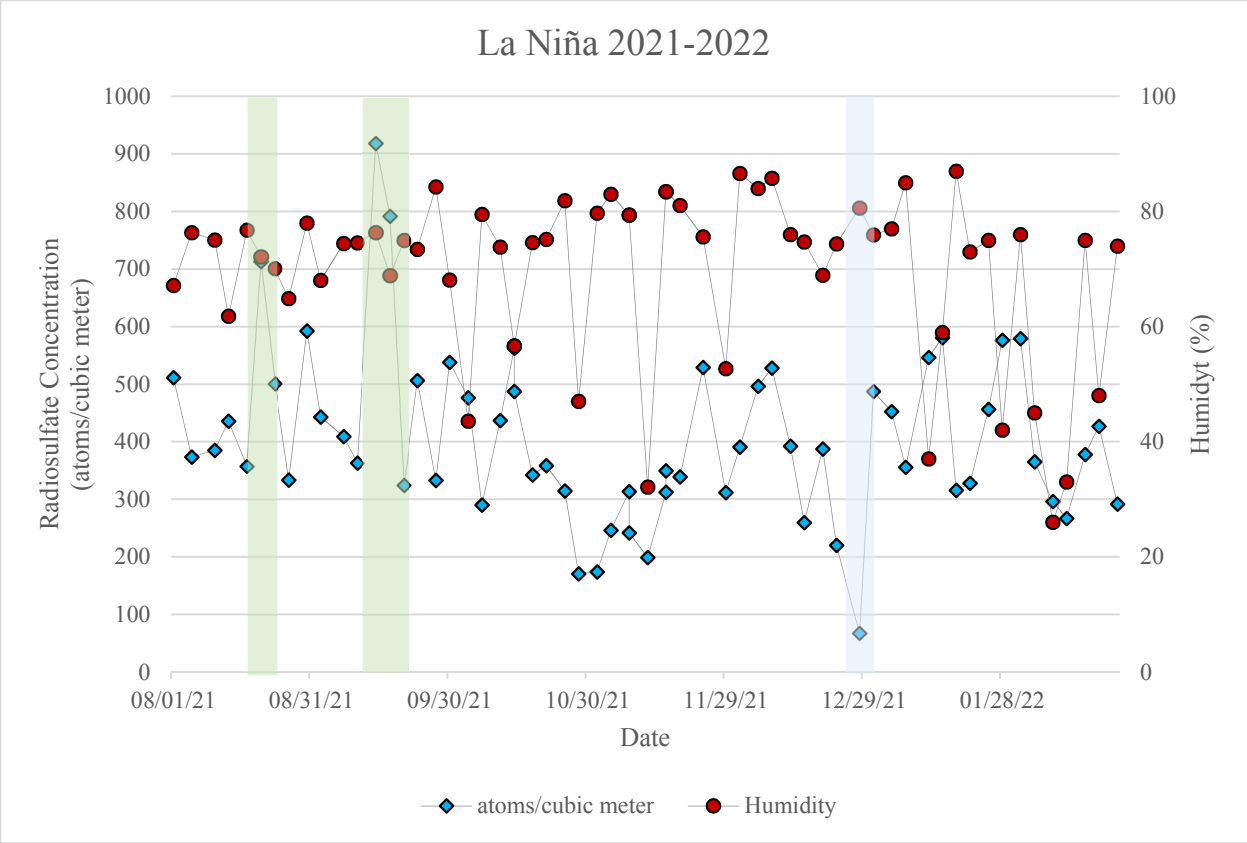

Figure 1.7 Bulk radiosulfate concentration and humidity plotted against date during LNSO Conditions 2021-2022. Instance highlighted where radiosulfate concentration exceeds 600 atoms m^{-3}.

LNSO 2021-2022 did not contain a higher frequency of STT events which may be characteristic of a weaker secondary LNSO as can be noted from Figure 1.2. Referencing back to Figure 1.2 it is observed that a maximum ONI value for the subsequent LNSO event was -1˚C, a value less than the -1.3˚C maximum ONI value for the initial LNSO event. Humidity fluctuations during this second LNSO were also more drastic with several instances of >80% and <60% humidity but did not demonstrate similar spikes in radiosulfate concentrations as can be seen during LNSO 2020-2021. A significantly low value present on 12/29 could be indicative of rainout or low sunspot number which will be further discussed in a later section.

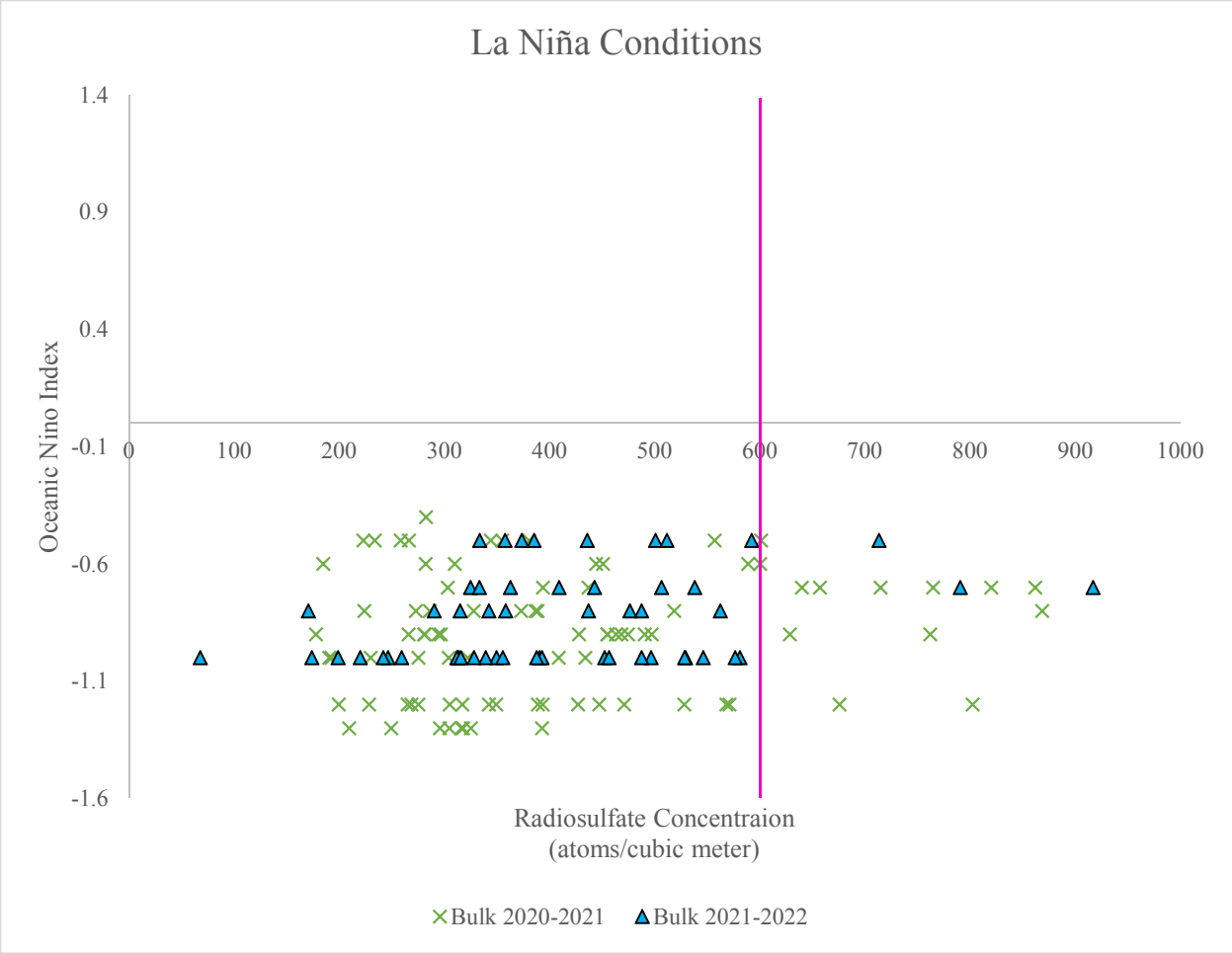

Figure 1.8 Bulk radiosulfate concentration vs ONI during LNSO 2020-2021 and LNSO 2021-2022.

The frequency of events where concentration of radiosulfate was greater than 600 atoms m^{-3} during this "double-dip" LNSO event is disproportionately higher during the first La Niña than the second. When comparing the two sets of data, it is important to consider what the average humidity for the two time periods is to verify that the difference matches the decreased frequency of radiosulfate spikes. During LNSO 2020-2021 the average humidity was 62% while LNSO 2021-2022 produced an average humidity of 70%. Increased humidity is indicative of a weaker second LNSO and should therefore yield lower concentrations of radiosulfate likely due

to increases in washout which removes the radiosulfur from the atmosphere. La Niña provides conditions where dry air can be transported from the equatorial region poleward by Hadley cells and BDC so an increase in humidity could be indicative of a change in the temperature gradients creating LNSO events so we can infer that the system is weakening. Figure 1.8 shows a greater number of instances where radiosulfate concentration exceeded 600 atoms m^{-3} during the 2020-2021 LNSO than the 2021-2022 LNSO. These spikes in concentration of Bulk samples indicates a greater number of large sulfate aerosol particles (>1.5 μm) being transported to the region of collection. To verify that these instances of greater concentration are coming from higher altitudes, back trajectories of air masses were calculated for each instance using HYSPLIT Trajectory software available at NOAA Air Resource Laboratory. Figure 1.9 contains back trajectories for elevated concentrations of radiosulfate during non-ENSO conditions shown in Figure 1.4. The collection site (Urey Hall, La Jolla CA) is marked with a star and the flow of air mass can be traced backward from that origin showing the direction of flow. Each of these maps contains data for the respective day the sample was collected and support the proposition that these air masses sink down during high pressure events and are transported to the origin of collection by Santa Ana winds.

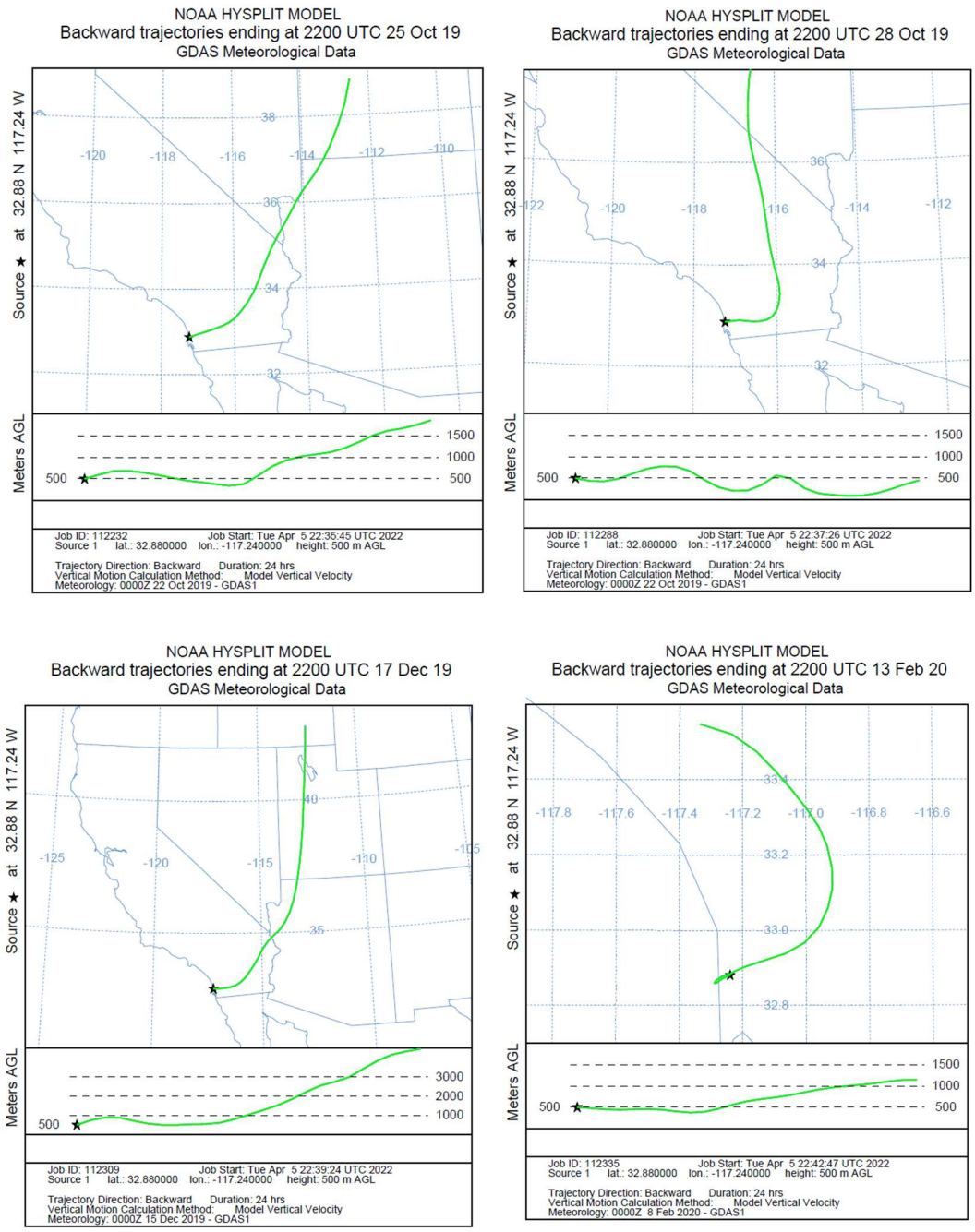

Figure 1.9 Back trajectories for spikes in radiosulfate during non-ENSO conditions as seen in Figure 1.4 calculated using NOAA Air Resource Laboratory HYSPLIT Program. The top plot shows the path of the air mass along the surface and the bottom plot shows the altitude of the sinking air mass.

Back trajectories were also calculated for samples collected during LNSO 2020-2021 and LNSO 2021-2022 where samples exceeded the 600 atoms m^{-3} to determine if the peaks were indeed due to STT events. Figure 1.10 contains back trajectories during La Niña 2020-2021 and Figure 1.11 contains back trajectories during La Niña 2021-2022.

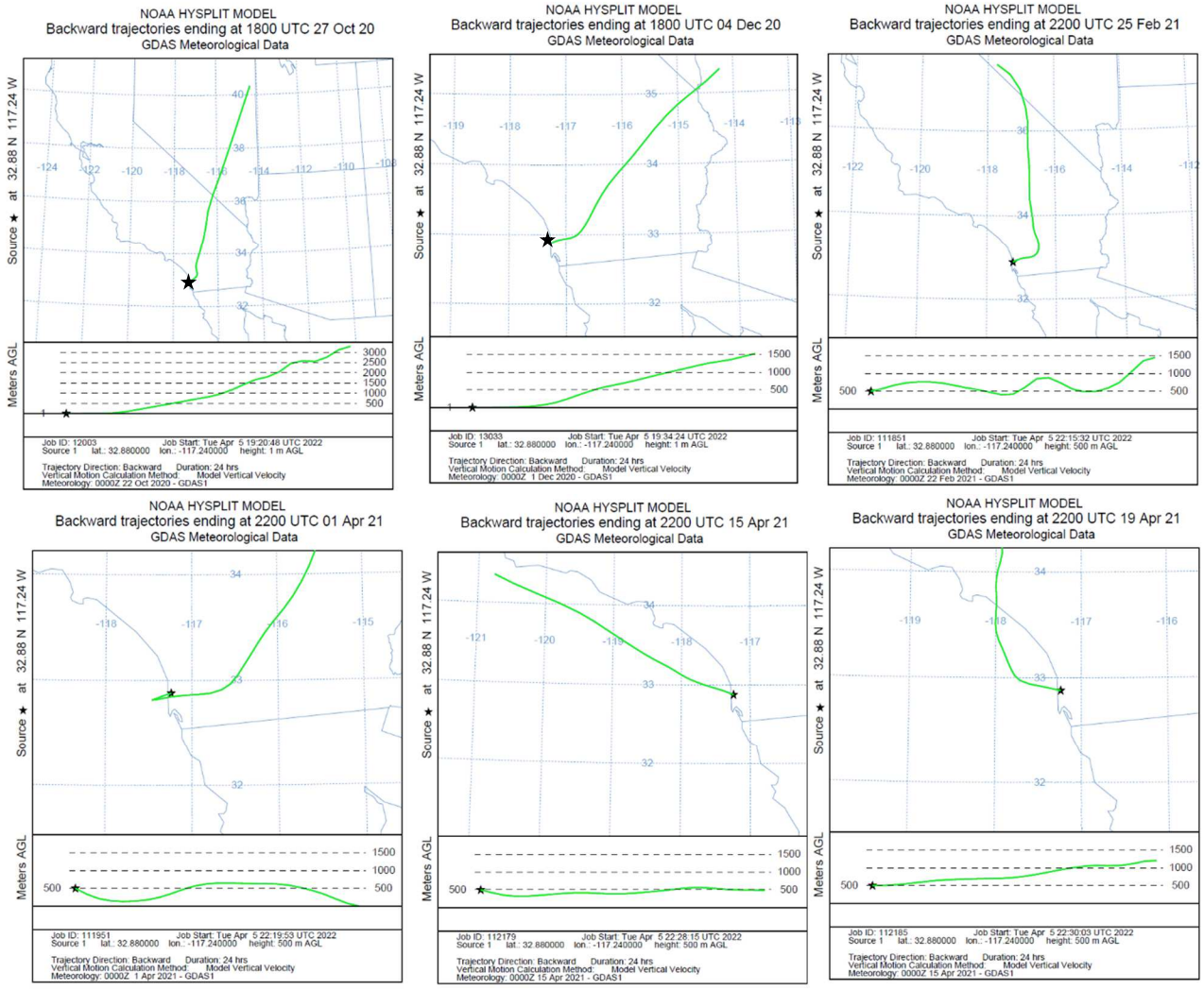

Figure 1.10 Back trajectories for spikes in radiosulfate during LNSO 2020-2021 as seen in Figure 1.5 calculated using NOAA Air Resource Laboratory HYSPLIT Program.

When analyzing the back trajectories shown in Figure 1.10, a majority of the anomalously high points during LNSO 2020-2021 can be attributed to STT events. Data

collected on April 1, 2021, appears to have travelled at much lower altitudes before being collected and data collected on April 15, 2021, travelled down from a northern high-pressure system also at much lower altitudes. These anomalies occurred during the end of La Niña 2020-2021 and may be indicative of the temperature equilibrium that is typically achieved as a LNSO approaches the end of its lifetime and conditions return to normal.

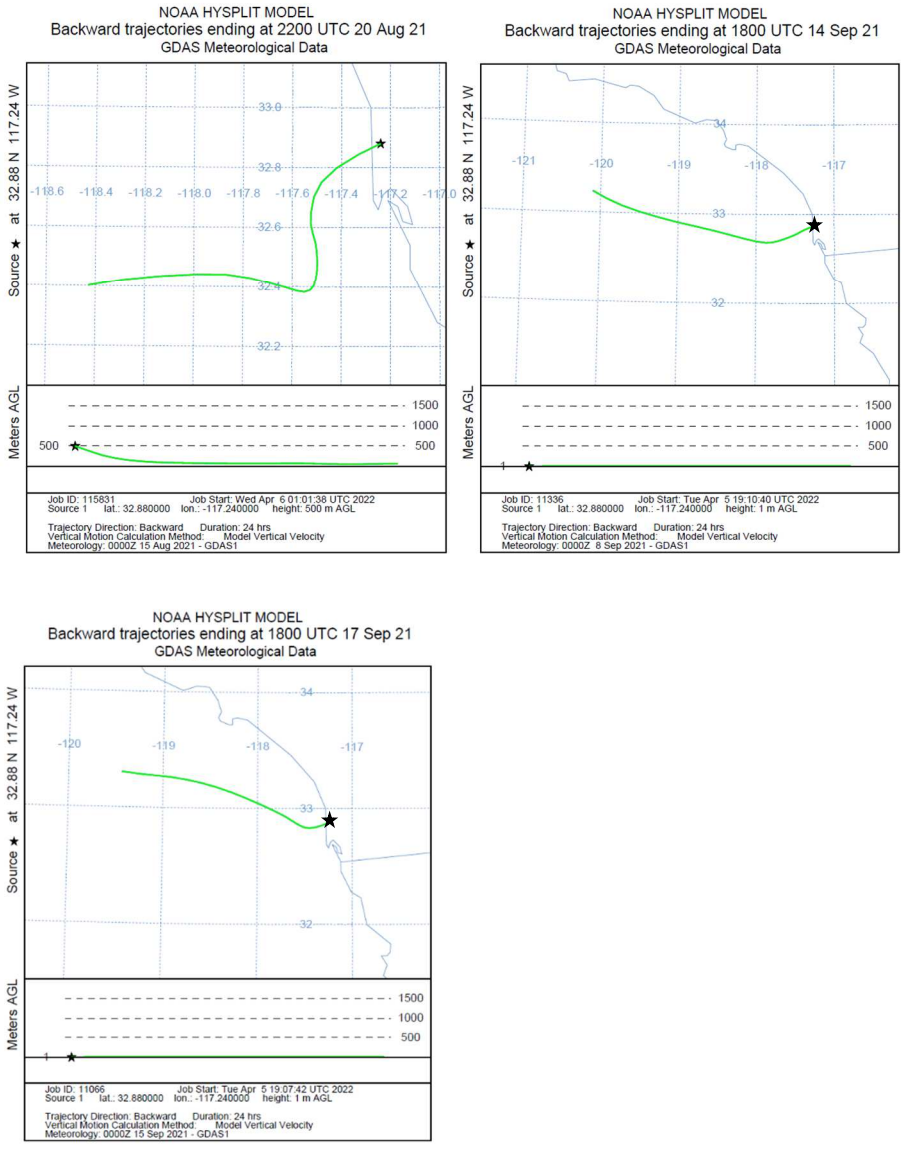

Figure 1.11 Back trajectories for spikes in radiosulfate during LNSO 2021-2022 as seen in Figure 1.7 calculated using NOAA Air Resource Laboratory HYSPLIT Program.

Examination of the back trajectories shown in Figure 1.11 show that the air masses corresponding to the anomalously high sulfate concentrations of LNSO 2021-2022 originated in a different location from those shown in Figure 1.10 and Figure 1.9. It is possible that the air masses shown in Figure 1.11 are travelling along the Subtropical Jet Stream. During a strong LNSO, the Polar Jet Stream shifts downward and dips across the United States between a region of high pressure and a region of low pressure that form over the western and eastern regions of the country respectively. It is likely that the Polar Jet Stream started to retreat poleward at the end of LNSO 2020-2021 and did not shift back downward for the second, weaker LNSO. This would have allowed the Subtropical Jet Stream to shift back up or reappear at its 30˚N location resuming flow from west to east over the Pacific Ocean (weather.gov). However, the altitude of origination for these air masses is lower than would be expected so it is important to consider the possibility of anthropogenic formation of ^{35}S which will be discussed further in a later section.

Considering the data that has thus far been presented it can be stated that given its short half-life and frequent transport, the cosmogenic ^{35}S tracer offers valuable uses as a real time indicator of present atmospheric and climactic changes. Understanding its behavior during complex weather phenomena such as LNSO can be of great use when studying the global sulfur cycle, the present ozone budget, and the negative impacts it has on human health as an aerosol pollutant. It can also provide earlier signs for developing changes in climate so that countries may better prepare for the dangerous effects that those changes might have on their economy and environment.

2.2 Observed Changes in Cosmogenic ^{35}S at Start of Solar Cycle 25's Solar Minimum

Understanding severe space weather is becoming increasingly important as it can greatly affect the function of satellites or the health of astronauts in outer space, especially with the rapidly expanding space flight frequency. Disruption of satellite-based communication, navigational networks, electric power grids, and even oil pipelines (control centers) by GCR is possible. Having the ability to understand or predict solar activity is increasingly important and may even be considered a priority concerning technological advancement (National Research Council, 1997, 2013; National Science and Technology Council, 2019; Krausmann et al., 2016; UNOOSA Space Weather, 2017; Schrijver et al., 2015). To reiterate, cosmogenic ^{35}S is produced by spallation of ^{40}Ar in the upper atmosphere and is rapidly oxidized to sulfur dioxide (~1 second) upon interaction with ozone, peroxide, or hydroxide. $^{35}SO_2$ can be removed from the atmosphere by dry and wet deposition but will typically undergo further oxidation to produce $^{35}SO_4^{2-}$. Except for anthropogenic sources, it can be stated that ^{35}S is produced in the upper atmosphere and is the only radioactive isotope that exists as an aerosol and a gas simultaneously. ^{35}S can act as a measure of solar activity since it is produced by solar flares or rare supernova explosions. Given that supernova explosions take place within the Milky Way every 50 years or so (Phillips, 2014) the production of ^{35}S will be attributed to solar flares produced by the sun. Cosmic rays from solar energetic particles, are composed mostly of high energy protons traveling at approximately the speed of light. Depending on the current state of the sun, at solar maximum or at solar minimum, rays will bombard Earth's atmosphere at different rates varying in intensity that result in different concentrations of ^{35}S in the upper atmosphere. At solar maximum there is a strong solar magnetic field present that contains GCR limiting the number of interactions with Earth's atmosphere leading to lower production rates of cosmogenic ^{35}S. In

contrast, at solar minimum there is a weakened solar magnetic field present that allows GCR to reach Earth's upper atmosphere and increase productions rates of cosmogenic ^{35}S.

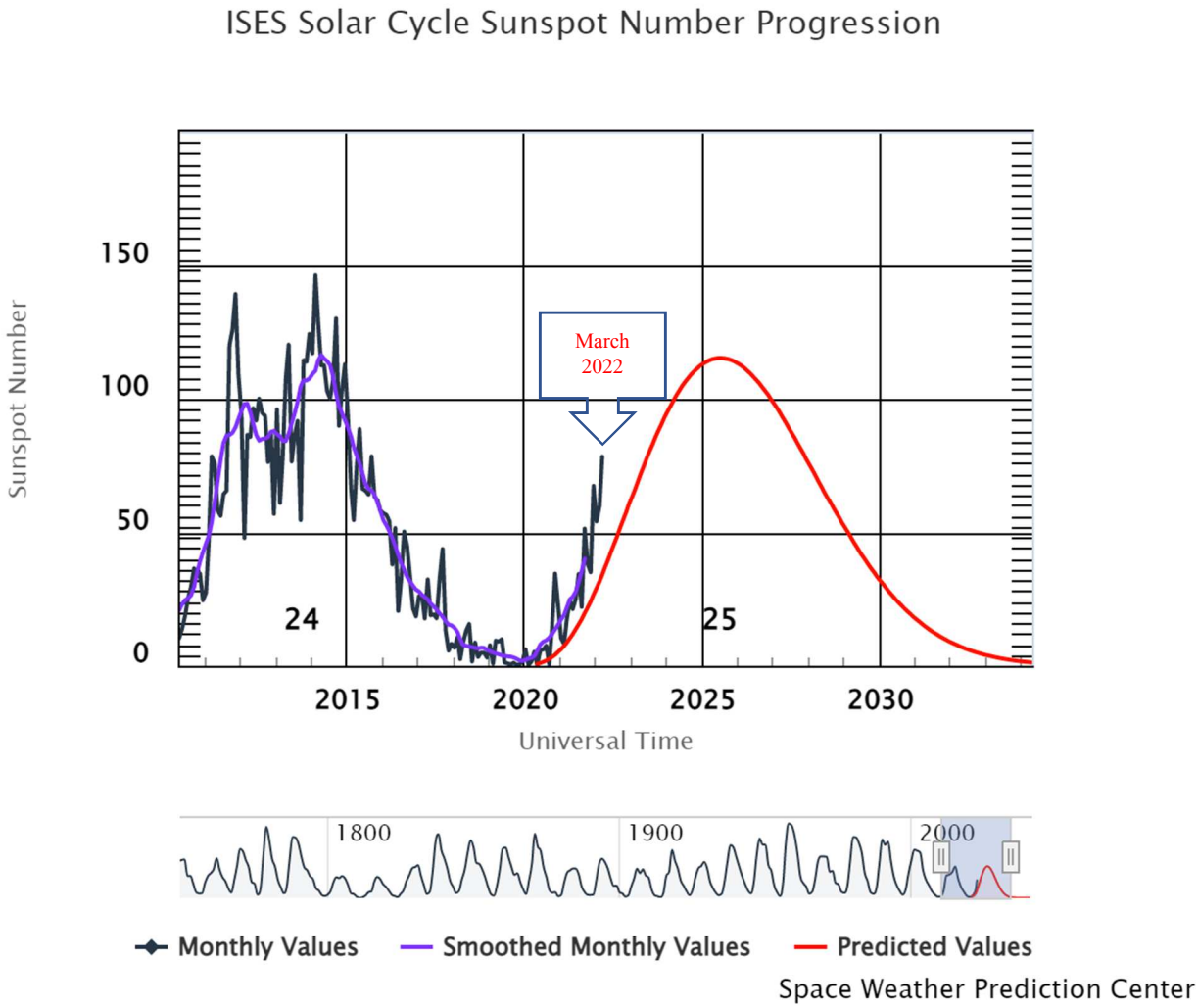

Figure 1.12 Transition period between Solar Cycle 24 and Solar Cycle 25. Predicted values for solar cycle 25 appear to be lower than the actual values being detected signifying a rapid approach to solar maximum (Space Weather Prediction Center, NOAA).

Solar Cycle 25 began at the lowest point of the solar minimum, as can be seen in Figure 1.12, spanning into solar cycle 24 and marking its end. According to this plot generated by Space Weather Prediction Center at NOAA, the maximum of solar cycle 25 is approaching much sooner than was forecasted. Due to this rapid shift in trajectory, we can expect to see lower

concentrations of fine and bulk radiosulfate as the number of sunspots continue to increase and the solar magnetic field strengthens. This supports the prediction that concentrations of bulk and fine sulfate aerosol will be higher during the solar minimum than would be during solar maximum as a result of the changing solar magnetic field between the two phases.

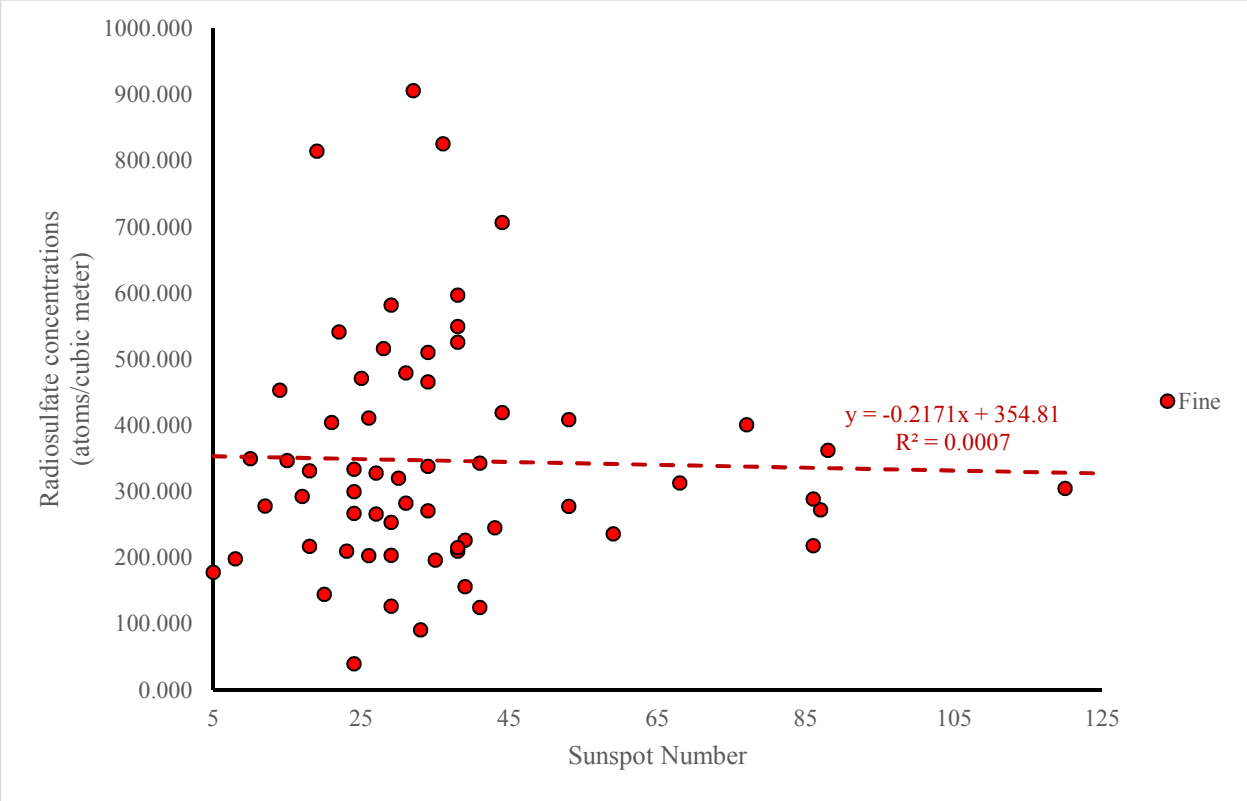

Figure 1.13 Fine radiosulfate concentrations plotted against respective sunspot number. Data collection presented from September 2019 to February 2020 resuming on October 2021 and ongoing. More instances of greater radiosulfate concentration are observed at lower sunspot numbers.

High concentrations of fine radiosulfate seen in Figure 1.13 correspond to lower sunspot numbers which demonstrates a relationship between solar activity and radiosulfate activity. Due to a decreased solar magnetic field during solar minimum, GCR are more likely to penetrate the

geomagnetic field of the earth and reach the upper atmosphere resulting in a greater number of spallation events.

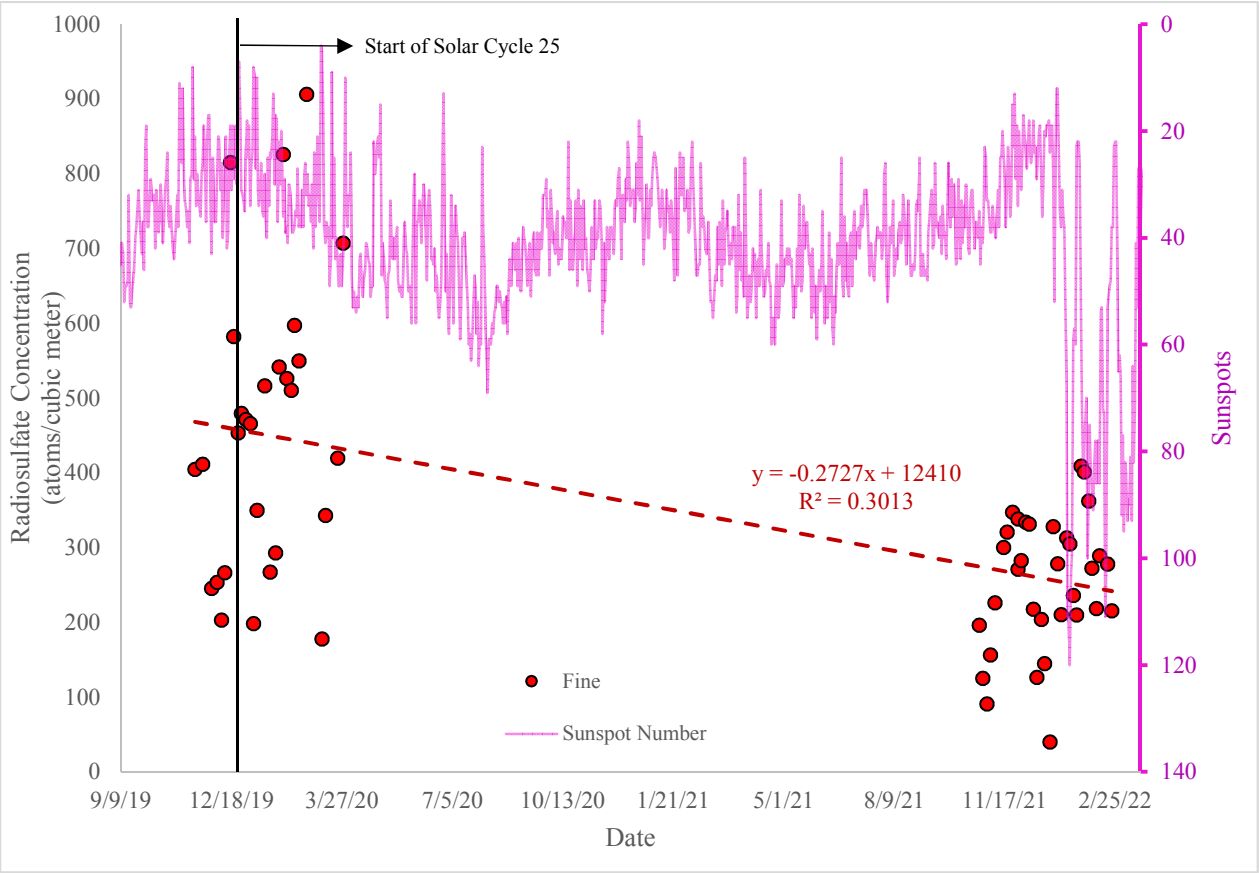

Figure 1.14 Fine radiosulfate concentration and sunspot number plotted against date beginning September 2019 to February 2020 resuming October 2021 and ongoing. Fine radiosulfate collected from 2019 to 2020 was higher in concentration at solar minimum while samples collected beginning October 2021 are lower in concentration as sunspot numbers begin to incline.

A greater number of spallation events would lead to increased concentrations of ^{35}S in the upper atmosphere consequently increasing the concentration of sulfate aerosol in the atmosphere.

The average sulfate concentration at the trough of the solar minimum between cycle 24 and 25 was 457 atoms m^{-3} (2019-2020), in agreement with the 2009-2010 average of 455±157 molecules m^{-3} (Priyadarshi et al, 2012). The recent rapid increase in sunspot number has an associated decreased radiosulfate concentration to 254 atoms m^{-3} (2021-present). This decrease in concentration indicates that the cycle is shifting form solar minimum to maximum as seen in Figure 1.12 confirming that the cycle is ramping up quicker than predicted.

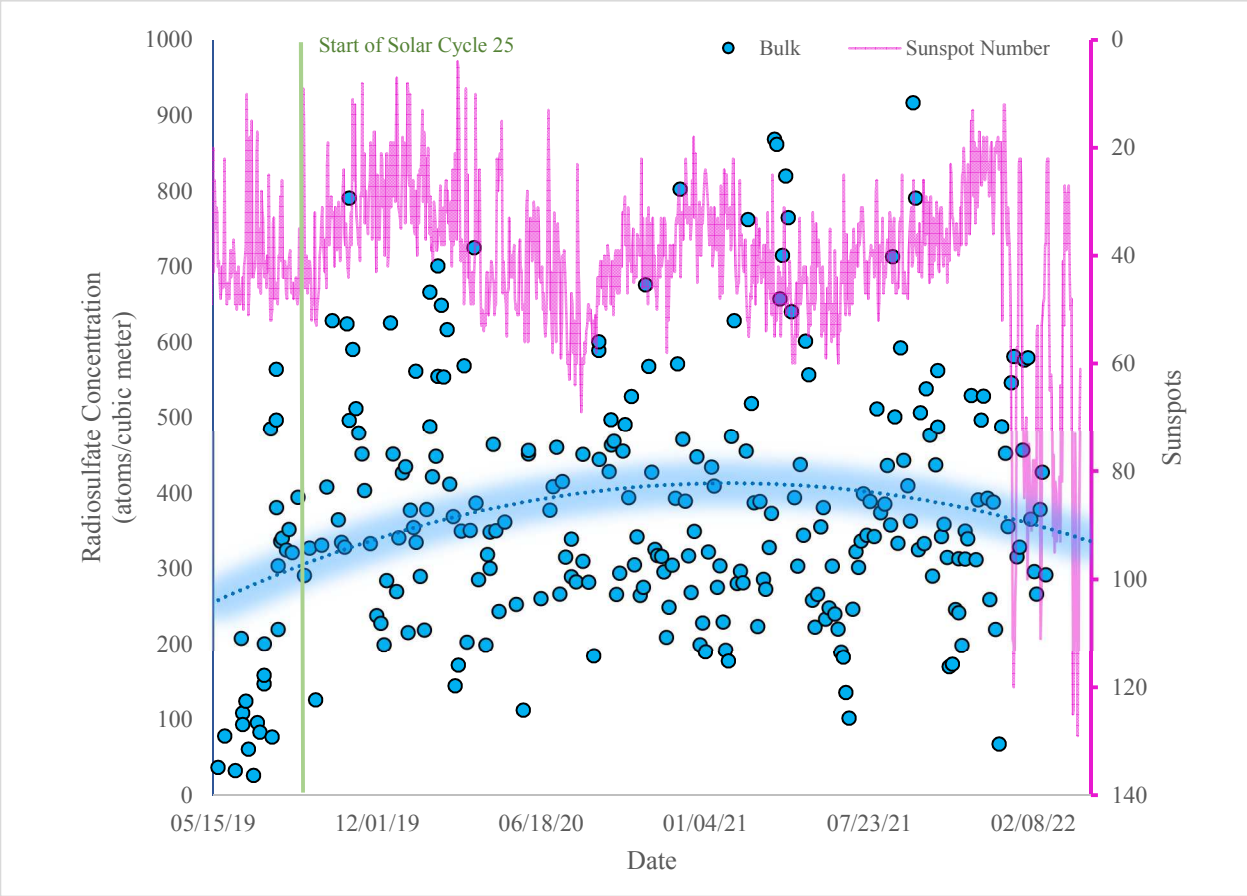

Figure 1.15 Bulk radiosulfate concentration and sunspot number plotted against date beginning May 2019. An inverse relationship between solar cycle activity and bulk radiosulfate concentration is apparent.

An inverse relationship between solar cycle activity and bulk radiosulfate concentration can be seen in Figure 1.15. Comparing the behavior of bulk particulate (>1.5 μm) to fine particulate (<0.95 μm), we can see that there is still an inverse relationship between bulk radiosulfate concentration and solar activity but less resolute than the inverse relationship between fine radiosulfate and solar activity. This inverse relationship is consistent with solar modulation of its magnetic field during solar minimum and maximum and thus controls the production of radionuclides in earth's upper atmosphere (Heaton et al, 2021 Poluianov et al, 2016).

This study includes analysis of ^{35}S during the extreme climatic variability of LNSO and turbulent atmospheric conditions of Santa Ana winds during non-ENSO conditions that occurred during a solar cycle shift. This data highlights the sensitivity of ^{35}S during radical changes in climate while still maintaining the integrity of information regarding solar activity making it an incredibly versatile tracer with an ideal half-life.

2.3 Anthropogenic ^{35}S: A Unique Traceable Indicator of Neutron Leakage

In this portion of the study, a long-term detection method of anthropogenic ^{35}S will be discussed as it pertains to nuclear waste storage facilities or nuclear power generating stations around the country.

Monitoring for anthropogenic ^{35}S can be carried out in conjunction with data collection for cosmogenic ^{35}S. Aerosol sulfate particulate originating from anthropogenic sources would be collected on air sample filters along with cosmogenic radiosulfate. Upon detection of abnormal levels of ^{35}S in an air sample, a series of discriminatory checks would be considered in order to determine the true origin of the sample. Primarily the abnormal sample would be recounted in order to verify that the reading is accurate thus ruling out the possibility of any human or technological error. Upon recounting, if the sample is consistent with the initially high reading, it will move on to the second check comparing it to historical values for the dates of sample collection. If records indicate that the time frame of collection is consistent with rare STT events or strong Santa Ana wind events, a back trajectory using NOAA HYSPLIT technology will be calculated to obtain the origin of the air mass to confirm. Air masses originating from stratospheric altitudes are likely to entrain large concentrations of newly produced cosmogenic radiosulfate which could produce an abnormally high signal when counted. Confirmation of an air mass coming from high altitude would rule out the possibility of an anthropogenic source and attribute the abnormally high signal to STT events or Santa Ana winds. Air masses that originate at low tropospheric altitudes would be indicative of anthropogenically produced radiosulfate and therefore stipulate the presence of fast or thermal neutron flux. If discrepancy exists when comparing the abnormally high reading to historical values, a back trajectory using HYSPLIT will be calculated in order to verify the origin of the air mass as previously explained. An

abnormally high sample that has been confirmed to have originated at low tropospheric altitudes will be further investigated using public radiation monitoring data along the travel path of the calculated air mass. If a known possible source of neutrons lies along the passage of the air mass, such as SONGS or Diablo Canyon lie along the coast of California, investigation of recent activity at the source could reveal evidence for possible neutron leakage.

Earlier in the study, back trajectories for spikes in radiosulfate during LNSO 2021-2022 were shown in Figure 1.11 to have originated at questionably low altitudes. It was discussed that the abnormal levels of radiosulfate were possibly transported to the collection site via the Subtropical Jet Stream, but the risk of anthropogenic origination must further be investigated due to the low originating altitude of the single air mass. To investigate the likelihood of an anthropogenic source, back trajectories over a broad time period (96 hours), which encompass the sample date, were calculated for each of the three outliers. Figure 1.16 contains three 96-hour back trajectories for the abnormal spikes in radiosulfate detected during LNSO 2021-2022.

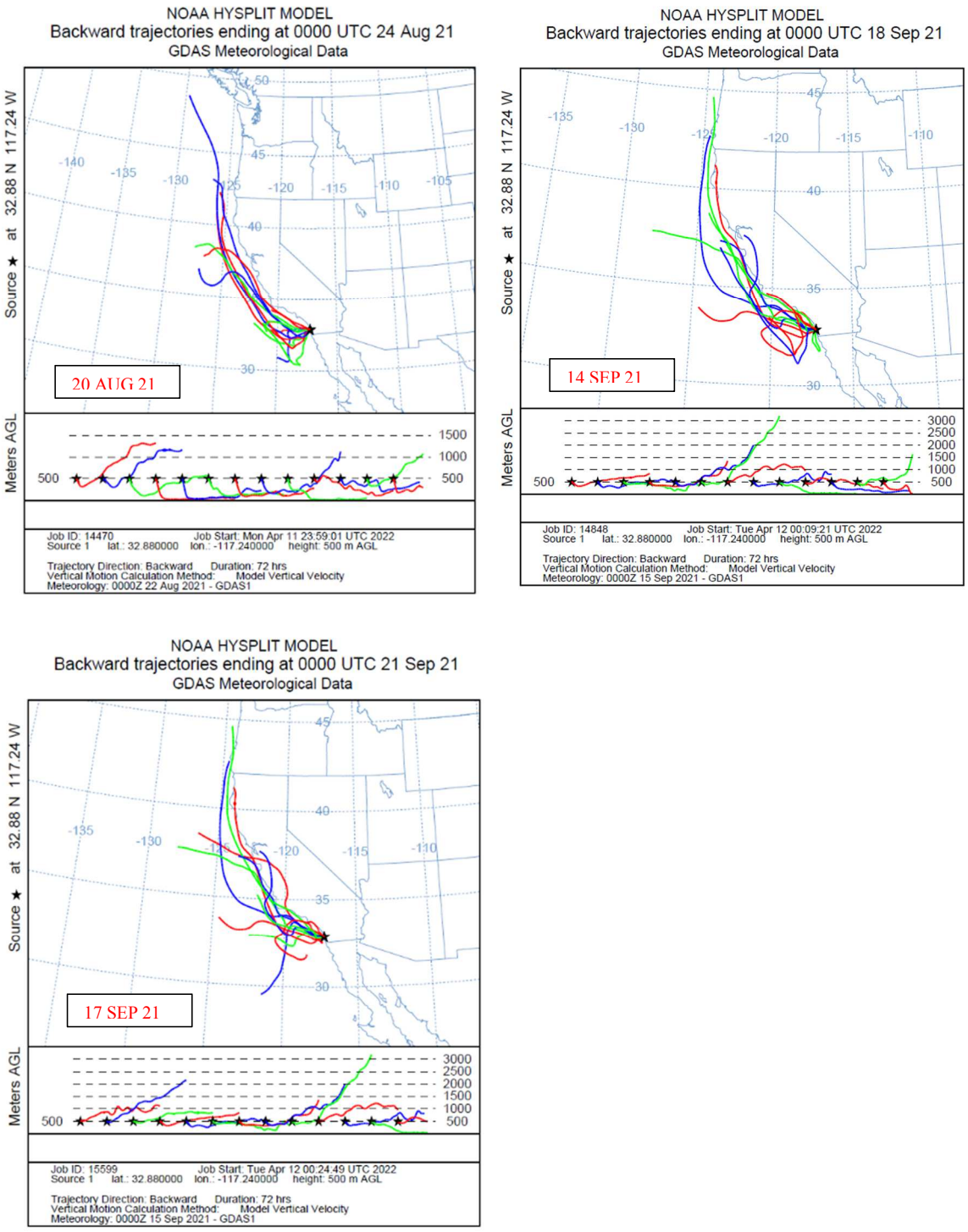

Figure 1.16 Broad (96 hour) back trajectories for spikes in radiosulfate during LNSO 2021-2022 referencing Figure 1.11 calculated using NOAA Air Resource Laboratory HYSPLIT Program.

After analyzing the 96-hour trajectories in Figure 1.16 it is most likely that the abnormal concentrations obtained on September 14, 2021, and September 17, 2021, were caused by northern STT events. Each of these two back trajectories contains an air mass emerging at >3km showing greater likelihood of STT influence rather than anthropogenic origin. The 96-hour back trajectory corresponding to the spike noted on August 20, 2021, contains few air masses which originated at >1km therefore anthropogenic influences cannot be completely ruled out.

It is possible that low levels of thermal neutron flux arising from anthropogenic sources, such as nearby nuclear power facilities, may be participating in slow neutron capture with ^{35}Cl contributing to existing levels of ^{35}S in each sample. For this reason, long term monitoring of $^{35}SO_4^{2-}$ aerosol combined with air mass transport technology can be useful in detecting early signs of neutron leakage from known radioactive sources.

Speculation of a different source of neutron flux was considered but a lack of literature makes it difficult to confirm with certainty that these vessels are contributing to the production of anthropogenic $^{35}SO_4^{2-}$. The restrictions and frequency for radioactive discharges authorized 12 nautical miles out from shore are not available for public access.

Chapter 3 Materials and Methodologies

3.1 Aerosol Sample Collection

Aerosol samples were collected at Urey Hall in La Jolla California (32.8˚N, 117.2˚W) using a high-volume air sampler (HVP-4300AFC, Hi-Q, U.S.) with a set flow rate of 40 standard ft^3 min^{-1}. Samples were collected on glass fiber filters (bulk and fine on Whatman GF/B; coarse on Tisch TE-230GF) with each sample spanning 4-5 days on average. Aerosol samples were size segregated to obtain bulk (>1.5 μm), coarse (<1.5 μm but >0.95 μm), and fine (<0.95 μm) samples using a cascade impactor (TE-234, Tisch, U.S.). Filter papers containing bulk and fine samples were cut into equal halves in order to archive half of the filter for future analysis or as support in case of human error.

3.2 Sulfate Extraction and Purification

The sample purification procedure adhered to optimized low-level liquid scintillation protocol described by Brothers et al (2010) and Lin et al (2017b). Half filters containing bulk and fine aerosol samples were carefully folded and placed into 50 ml centrifuge tubes (Fisherbrand™) each. Filters were immersed in ~25 ml Milli-Q deionized water (18 MΩ cm) and sonicated for 60 minutes. Dissolved sulfate is separated from the filter by inserting a Buchner funnel into a clean 50 ml centrifuge tube, quantitatively transferring ~25 ml Milli-Q deionized water containing sulfate and centrifuging the apparatus for 10 minutes. The filter itself is then inserted into the Buchner funnel and centrifuged for 16 minutes to extract remaining dissolved sulfate. Finally, a 10 ml rinse of Milli-Q deionized water is added to the filter in the Buchner funnel and centrifuged for a final 18 minutes in order to maximize sulfate extraction. After each centrifugation, extracted sulfate is quantitatively transferred to a 50 ml centrifuge tube where the

final volume extracted averages at ~35 ml. To the extracted sample, 10 ml of H_2O_2 (30% Certified ACS Grade, Fisher Scientific) is added and dried in a clean oven for 24 hours. Reduced sulfur compounds that exist in the condensed phase are negligible compared to sulfates in the sample (Lin et al, 2017a) so there would be no negative impact on the accurate determination of ^{35}S concentration in aerosol sulfate due to the use of H_2O_2. Completely dry samples are removed from the oven and rehydrated with 2 ml Milli-Q deionized water followed by 60 minutes of sonication to encourage maximum dissolution of sulfate. Redissolved sulfate samples were purified by one polyvinylpyrrolidone (PVP) column followed by an IC-Ag cartridge (Dionex OnGuard II) followed by a second polyvinylpyrrolidone (PVP) column. The initial 2 ml resuspended sample is run through the first PVP column followed by a 2 ml Milli-Q deionized water rinse of the 50 ml tube. Total of 4ml are then run through the IC-Ag cartridge and the second PVP column. A final 1 ml rinse of Milli-Q deionized water is added to the 50 ml centrifuge tube and centrifuged for 4 minutes before being run through the first PVP column, IC-Ag cartridge, and the second PVP column. A total of 5 ml of sample is collected into a 15 ml centrifuge tube (Fisherbrand™) to which 2 ml H_2O_2 is added to extract any final organic impurities.

3.3 Ultra-Low-Level Liquid Scintillation Counting

Purified sulfate samples are quantitatively transferred to 20 ml plastic scintillation vials (Fisherbrand™) and mixed with 10 ml of scintillation gel (Ultima Gold, PerkinElmer). The use of this particular scintillation cocktail eliminates the possible interference of radionuclide interference common in barium reagents thus allowing for clear counting of ^{35}S (Brothers et al, 2010) in quantities <1.5 mmol (Lin et al, 2017b). Using an Ultra-Low-Level Liquid Scintillation

Counting Spectrometer (Quantulus 1220, PerkinElmer) following the procedure delineated by Brother et al (2010). Keeping in mind that possible contamination from ^{14}C may exist, channels 1-450 were selected in order to minimize interference from ^{14}C while focusing on a peak at ~300 for radiosulfate (Brothers et al, 2010). Each sample is counted 6 times, 2 hours at a time, and the average of those 6 counts is taken and used for data analysis. Each sample is checked for possible phase separation, bubbles, or pigmentation before and after counting as these factors could interfere with ^{35}S counting efficiency.

References

Adamson, G., 2020, IMPERIAL OSCILLATIONS: Gilbert Walker and the Construction of the Southern Oscillation, *Weather, Climate, and the Geographical Imagination: Placing Atmospheric Knowledges*. Mahony, M. & Randalls, S. (eds.). University of Pittsburgh Press, p. 43-66, https://doi.org/10.2307/j.ctv10h9g13.6

Brothers, L. A., G. Dominguez, A. Abramian, A. Corbin, B. Bluen, and M. H. Thiemens (2010), Optimized low-level liquid scintillation spectroscopy of S-35 for atmospheric and biogeochemical chemistry applications, P Natl Acad Sci USA, 107(12), 5311-5316, Doi: Doi 10.1073/Pnas.0901168107.

Butchart, N. (2014). The brewer□Dobson Circulation. *Reviews of Geophysics*, *52*(2), 157–184. https://doi.org/10.1002/2013rg000448

Castelvecchi, D. (2022). Ukraine Nuclear Power Plant Attack: Scientists assess the risks. *Nature*. https://doi.org/10.1038/d41586-022-00660-z

Center, N. O. A. A. C. P. (2001, January 1). *NOAA's Climate Prediction Center*. Climate Prediction Center. Retrieved April 13, 2022, from https://origin.cpc.ncep.noaa.gov/products/analysis_monitoring/ensostuff/ONI_v5.php#:~:text=The%20ONI%20is%20one%20measure%20of%20the%20El,with%20a%20coupled%20ocean-atmosphere%20phenomenon%20accompanied%20these%20periods.

Chang, P., & Zebiak, S. E. (2003). EL NIÑO AND THE SOUTHERN OSCILLATION | Theory. *Encyclopedia of Atmospheric Sciences*, 719–724. https://doi.org/10.1016/b0-12-227090-8/00149-4

Corporation, V. C. (n.d.). *Weather Data Services: Visual Crossing*. Weather Data Services | Visual Crossing. Retrieved April 13, 2022, from https://www.visualcrossing.com/weather/weather-data-services

DiNezio, P. N., Deser, C., Karspeck, A., Yeager, S., Okumura, Y., Danabasoglu, G., Rosenbloom, N., Caron, J., & Meehl, G. A. (2017). A 2-year forecast for a 60–80% chance of La Niña in 2017–2018. *Geophysical Research Letters*, *44*(22). https://doi.org/10.1002/2017gl074904

Fu, Q., Solomon, S., Pahlavan, H. A., & Lin, P. (2019). Observed changes in Brewer–Dobson circulation for 1980–2018. *Environmental Research Letters*, *14*(11), 114026. https://doi.org/10.1088/1748-9326/ab4de7

Heaton, T. J., Bard, E., Bronk Ramsey, C., Butzin, M., Köhler, P., Muscheler, R., Reimer, P. J., & Wacker, L. (2021). Radiocarbon: A key tracer for studying Earth's dynamo, climate system, carbon cycle, and sun. *Science*, *374*(6568). https://doi.org/10.1126/science.abd7096

Kentarchos, A. S. (2003). A model study of stratospheric ozone in the troposphere and its contribution to tropospheric oh formation. *Journal of Geophysical Research*, *108*(D12). https://doi.org/10.1029/2002jd002598

Kirpes, R. M., Lei, Z., Fraund, M., Gunsch, M. J., May, N. W., Barrett, T. E., Moffett, C. E., Schauer, A. J., Alexander, B., Upchurch, L. M., China, S., Quinn, P. K., Moffet, R. C., Laskin, A., Sheesley, R. J., Pratt, K. A., & Ault, A. P. (2022). Solid organic-coated ammonium sulfate particles at high relative humidity in the summertime Arctic atmosphere. *Proceedings of the National Academy of Sciences*, *119*(14). https://doi.org/10.1073/pnas.2104496119

Krausmann, E., Andersson, E., Murtagh, W., Gibbs, M.: 2016, *Space Weather & Critical Infrastructures: Findings and Outlook*. DOI

Lau, K.-M., & Yang, S. (2003). Walker circulation. *Encyclopedia of Atmospheric Sciences,* 2505–2510. https://doi.org/10.1016/b0-12-227090-8/00450-4

Liberto, T. D. (2014, August 1). The Walker Circulation: ENSO's atmospheric buddy. Retrieved April 13, 2022, from https://www.climate.gov/news-features/blogs/enso/walker-circulation-ensos-atmospheric-buddy.

Lin, C. Y., F. Chen, J. C. Huang, W. C. Chen, Y. A. Liou, W. N. Chen, and S. C. Liu (2008a), Urban heat island effect and its impact on boundary layer development and land-sea circulation over northern Taiwan, Atmos Environ, 42(22), 5635-5649.

Lin, M., S. Biglari, Z. Zhang, D. Crocker, J. Tao, B. Su, L. Liu, and M. H. Thiemens (2017b), Vertically uniform formation pathways of tropospheric sulfate aerosols in East China detected from triple stable oxygen and radiogenic sulfur isotopes, Geophys Res Lett.

Lin, M., Su, L., Shaheen, R., Fung, J. C., & Thiemens, M. H. (2016). Detection of deep stratospheric intrusions by cosmogenic 35 S. *Proceedings of the National Academy of Sciences*, *113*(40), 11131–11136. https://doi.org/10.1073/pnas.1609919113

Lin, M., & Thiemens, M. H. (2022). Cosmogenic radiosulfur tracking of solar activity and the strong and long-lasting El Niño events. *Proceedings of the National Academy of Sciences*.

Lindzen, Richard S., and Brian Farrell. "The role of polar regions in global climate, and a new parameterization of global heat transport." *Monthly Weather Review* 108 (1980): 2064-2079.

Love, D. L., and D. Sam (1962), Radiochemical determination of sodium- 24 and sulfur-35 in seawater, Anal. Chem., 34(3), 336–340.

National Research Council: 1997, *Space Weather: A Research Perspective*, The National Academies Press, Washington. DOI.

National Research Council: 2013, *Solar and Space Physics: A Science for a Technological Society*, The National Academies Press, Washington. ISBN 978-0-309-16428-3. DOI.

National Science and Technology Council: 2019, *National Space Weather Strategy and Action Plan*, The White House Office of Science and Technology, Washington. https://www.whitehouse.gov/wp-content/uploads/2019/03/National-Space-Weather-Strategy-and-Action-Plan-2019.pdf.

Nikolewski, R. (2019, July 27). Finding a repository for San Onofre plant's nuclear waste is a difficult task. *Los Angeles Times*.

Philander, S. G. H. (1985). El Niño and La Niña. *Journal of the Atmospheric Sciences*, *42*(23), 2652–2662. https://doi.org/https://doi.org/10.1175/1520-0469(1985)042<2652:ENALN>2.0.CO;2

Phillips, T. (2014, August 26). *Evidence for supernovas near earth*. NASA. Retrieved April 13, 2022, from https://science.nasa.gov/science-news/science-at-nasa/2014/26aug_localbubble/?msclkid=aa030532b69411ecacad715bc3669718

Price HU, Jaffe DA, Cooper OR, Doskey PV (2004) Photochemistry, ozone production, and dilution during long-range transport episodes from Eurasia to the northwest United States. J Geophys Res 109: D23S13.

Priyadarshi, A., Domínguez, G., & Thiemens, M. H. (2011). Evidence of neutron leakage at the Fukushima nuclear plant from measurements of radioactive 35S in California. *Proceedings of the National Academy of Sciences*, *108*(35), 14422–14425. https://doi.org/10.1073/pnas.1109449108

Priyadarshi, A., Hill-Falkenthal, J., Coupal, E., Dominguez, G., Thiemens, M. H., Measurements of S-35 in the marine boundary layer at La Jolla, California: A new technique for tracing air mass mixing during Santa Ana events. J Geophys Res-Atmos 117, D08301 (2012).

Poluianov, S. V., Kovaltsov, G. A., Mishev, A. L., & Usoskin, I. G. (2016). Production of cosmogenic isotopes7be,10be,14c,22na, and36cl in the atmosphere: Altitudinal profiles of yield functions. *Journal of Geophysical Research: Atmospheres*, *121*(13), 8125–8136. https://doi.org/10.1002/2016jd025034

Potter, S. (2021, January 4). *Solar cycle 25 is here. NASA, NOAA scientists explain what that means*. NASA. Retrieved April 13, 2022, from https://www.nasa.gov/press-release/solar-cycle-25-is-here-nasa-noaa-scientists-explain-what-that-means

Rahmanifard, F., Jordan, A. P., Wet, W. C., Schwadron, N. A., Wilson, J. K., Owens, M. J., Spence, H. E., & Riley, P. (2021). Evidence from Galactic Cosmic Rays that the Sun has likely entered a secular minimum in solar activity. *Space Weather*, *20*(2). https://doi.org/10.1029/2021sw002796

Rind, D. (1998). Latitudinal temperature gradients and climate change. *Journal of Geophysical Research: Atmospheres*, *103*(D6), 5943–5971. https://doi.org/10.1029/97jd03649

Robock, A. (2003). Volcanoes | role in climate. *Encyclopedia of Atmospheric Sciences*, 2494–2500. https://doi.org/10.1016/b0-12-227090-8/00448-6

Russell, G J, Todosow, M, Ferguson, P D, Kidman, R B, & Pitcher, E J. *Accelerator-driven targets: understanding and analyzing the spallation process*. United States.

Schrijver, C.J., Kauristie, K., Aylward, A.D., Denardini, C.M., Gibson, S.E., Glover, A., Gopalswamy, N., Grande, M., Hapgood, M., Heynderickx, D., Jakowski, N., Kalegaev, V.V., Lapenta, G., Linker, J.A., Liu, S., Mandrini, C.H., Mann, I.R., Nagatsuma, T., Nandy, D., Obara, T., Paul O'Brien, T., Onsager, T., Opgenoorth, H.J., Terkildsen, M., Valladares, C.E., Vilmer, N.: 2015, Understanding space weather to shield society: A global road map for 2015-2025 commissioned by COSPAR and ILWS. *Adv. Space Res.* **55**, 2745. DOI

Shaheen, R., Abauanza, M., Jackson, T. L., McCabe, J., Savarino, J., & Thiemens, M. H. (2013). Tales of volcanoes and El-Niño Southern oscillations with the oxygen isotope anomaly of sulfate aerosol. *Proceedings of the National Academy of Sciences*, *110*(44), 17662–17667. https://doi.org/10.1073/pnas.1213149110

Shaheen, R., Abaunza, M. M., Jackson, T. L., McCabe, J., Savarino, J., & Thiemens, M. H. (2014). Large sulfur-isotope anomaly in nonvolcanic sulfate aerosol and its implications for the Archean atmosphere. *Proceedings of the National Academy of Sciences*, *111*(33), 11979–11983. https://doi.org/10.1073/pnas.1406315111

Sims GHE, Juhnke DG (1969) The thermal neutron capture cross section and resonance capture integral of 35Cl for (n, .) and (n, p) reactions. J Inorg Nucl Chem 31:3721–3725.

Tanaka, N., and K. Turekian (1995), Determination of the dry deposition flux of SO2 using cosmogenic 35S and 7Be measurements, J. Geophys. Res., 100(D2), 2841–2848, doi:10.1029/94JD02305.

Tu FH, et al. (2004) Long-range transport of sulfur dioxide in the central Pacific. J Geophys Res 109: D15S08.

Turekian, K., and W. C. Graustein (2003), Natural radionuclides in the atmosphere, in Treatise on Geochemistry, pp. 261–279, Elsevier, Amsterdam, doi:10.1016/B0-08-043751-6/04042-1.

Unger, N., Shindell, D. T., Koch, D. M., Amann, M., Cofala, J., & Streets, D. G. (2006). Influences of man-made emissions and climate changes on tropospheric ozone, methane, and sulfate at 2030 from a broad range of possible futures. *Journal of Geophysical Research*, *111*(D12). https://doi.org/10.1029/2005jd006518

UNOOSA Space Weather: 2017, Special report of the inter-agency meeting on outer space activities on developments within the United Nations system related to space weather. http://www.unoosa.org/oosa/oosadoc/data/documents/2017/aac.105/aac.1051146_0.html.

Warf, B. (2010). Hadley Cell. In *Encyclopedia of geography* (pp. 1482–1397). essay, Sage Publications.